Journal of Materials Chemistry A

ROYAL SOCIETY OF CHEMISTRY

REVIEW

View Article Online
View Journal | View Issue

Cite this: J. Mater. Chem. A, 2023, 11, 21009

Liquid interfaces: an emerging platform for energy conversion and harvesting

Sai Zhao, [ab] Yuchen Fu,[ab] Haowu Cao[ac] and Yu Chai*[ab]

Energy conversion and harvesting technologies primarily rely on interface interactions at the liquid–liquid and liquid–solid interfaces. The efficient functioning of these technologies can be achieved through interface engineering, which regulates mass transfer and charge transportation. Several strategies have been employed to control the properties of the interface and enhance energy conversion efficiency. Significant progress has been made in understanding reactions at the liquid interface, opening new opportunities for its application. This review summarizes recent advancements in liquid interface manipulation methods, such as structured liquids and ultra-stable emulsions, and various liquid interface-based applications, including hydrovoltaic, triboelectric nanogenerators, all-liquid batteries, and water desalination, offering insights into the understanding of the complicated liquid interface and the reactions happening at liquid interfaces.

Received 27th June 2023
Accepted 4th September 2023

DOI: 10.1039/d3ta03760f

rsc.li/materials-a

1. Introduction

Liquid interfaces, including the liquid–liquid and liquid–solid interfaces, are essential platforms where chemical and physical reactions occur. These interfaces possess various fascinating features, such as their intrinsic negatively charged state and high-energy state, which allow us to carry out desired reactions.[1–4] For instance, by assembling functionalized nanoparticles at the liquid interface, we can form a structured liquid and modulate its shape and movement.[5–7]

In recent years, the global energy crisis has emerged as the major challenge faced by society. To tackle this, researchers have been developing low-cost and sustainable approaches to harvesting energy more efficiently. Energy conversion and storage technologies such as batteries have led to environmental pollution and resource depletion.[8] As a result,

[a]Department of Physics, The City University of Hong Kong, 83 Tat Chee Avenue, Kowloon, Hong Kong SAR 999077, China. E-mail: yuchai@cityu.edu.hk
[b]City University of Hong Kong Shenzhen Research Institute, 8 Yuexing First Road, Gaoxin District, Shenzhen 518057, China
[c]School of Physics and Technology, Wuhan University, Wuhan 430072, China

Sai Zhao is a PhD candidate at the City University of Hong Kong. He obtained his M. Eng in 2019 from the Beijing University of Chemical Technology. His research focuses on the self-assembly behaviors of nanomaterials at liquid interfaces and their applications in fabricating multi-functional nanocomposites and devices.

Dr. Yu Chai is an Assistant Professor of Physics at the City University of Hong Kong, where he joined the faculty in 2020. Prior to this, he was a Postdoctoral Researcher at the University of California, Berkeley, and Lawrence Berkeley National Laboratory. He received his PhD in Physics from the University of Waterloo. His research interests lie in the field of soft matter, with a particular focus on surfaces and interfaces. Through the utilization of cutting-edge in situ instruments, such as atomic force microscopes, he and his group have uncovered many intriguing behaviors exhibited by various soft materials at surfaces and interfaces, including the enhanced surface dynamics of glassy polymers, the self-assembly of nanomaterials at the liquid–liquid interface, and more.

alternative techniques, such as photo-thermal conversion and hydrovoltaics, have been developed.[9–12] It is noteworthy that liquid interfaces can and will play a crucial role in these applications.

In this review, we primarily focus on the recent research advances in using liquid interfaces as an emerging platform for energy conversion and harvesting (highly efficient catalysis,[13,14] nano-micro reactors,[15,16] self-propelled cargo,[17,18] electric generators,[19,20] *etc.*). In the first part of the review, we discuss the methods used to manipulate the properties of liquid interfaces. In the second part, we introduce emerging applications that involve liquid–liquid and liquid–solid interfaces for harvesting energy. Finally, we will provide an overview of the current challenges faced by liquid-interface-based energy conversion and harvesting approaches.

2. Manipulation of the liquid interface

2.1. Intrinsic properties of the liquid interface

2.1.1. Liquid–liquid interface. The interface between the two immiscible liquids is dominated by the inherent interfacial tension, γ, with units of N m^{-1} or J m^{-2}. Therefore, any change in the interfacial tension causes external forces or energies. For the liquid interface, free energy (G) can be expressed by eqn (1):

$$G = \gamma A \tag{1}$$

Interfacial tension is a fundamental property that governs the shape and area of the interface between two different phases. It tends to minimize the free energy of the system by pulling the interface into the shape that has the least amount of surface area. For a non-flat interface, the pressure included by the interfacial tension and local curvature can be described by the Young–Laplace eqn (2):[21]

$$\Delta p = \gamma\left(\frac{1}{R_1} + \frac{1}{R_2}\right) \tag{2}$$

where Δp is the pressure difference across the fluid interface, and R_1 and R_2 are the principal radii of curvature of the interface.

Interfacial tension is an intrinsic property of a two-liquid interface that remains constant under a given condition. However, by introducing materials favorable to both liquids, such as spherical amphiphilic nanoparticles, the spontaneous adsorption of these materials onto the liquid interface can reduce the interfacial tension. For instance, at a water–oil interface, the reduction in interfacial energy (ΔE) induced by the absorption of an ideal spherically shaped particle (*i.e.*, with spherical geometry and homogeneous surface chemistry) can be estimated as follows:[22]

$$\Delta E = \pi R^2 \gamma_{ow}(1 - |\cos\theta|)^2 \tag{3}$$

where R is the radius of the nanoparticle and θ is the contact angle (CA) at the three-phase contact line, as shown in Fig. 1a.

Various interfacially active materials have been developed based on these principles to alter the interfacial tension, thereby manipulating liquid interfaces. For instance, surfactants can be created by terminating polymers with hydrophilic functional groups.[23–25] These amphiphilic polymer surfactants can spontaneously attach to the water–oil interface, reducing the interfacial tension and serving as emulsifiers to create emulsions, which have been used in many areas, including the food industry, biomedicine, cosmetics industry,[26–28] *etc.*

Janus particles, which have two distinct geometries or chemical properties, have been reported to reduce the interfacial tension and effectively stabilize Pickering emulsions.[29] The asymmetric properties of Janus particles allow each distinct part to preferentially interact with its preferred phase, resulting in a strong absorption energy that dominates over thermal energy. Yang and colleagues have developed a range of efficient Janus particles, including block copolymers and inorganic Janus particles, that can be used to stabilize Pickering emulsions.[30–32]

In addition to energy, the inherent negative charges at the water–oil interface also provide opportunities to manipulate the liquid interface in different ways. The negative charge of the interface is believed to come from the adsorption of hydroxyl ions, which is independent of the oil type.[1] By introducing positively charged nanoparticles, attractive interaction occurs between the charged nanoparticles and the interface, allowing the nanoparticles to absorb onto the interface. This has inspired researchers to introduce other types of interactions, such as electrostatic interactions[33,34] and host–guest recognition,[5,35] to achieve interfacial assembly more efficiently. Russell and co-workers reported the self-assembly of positively charged

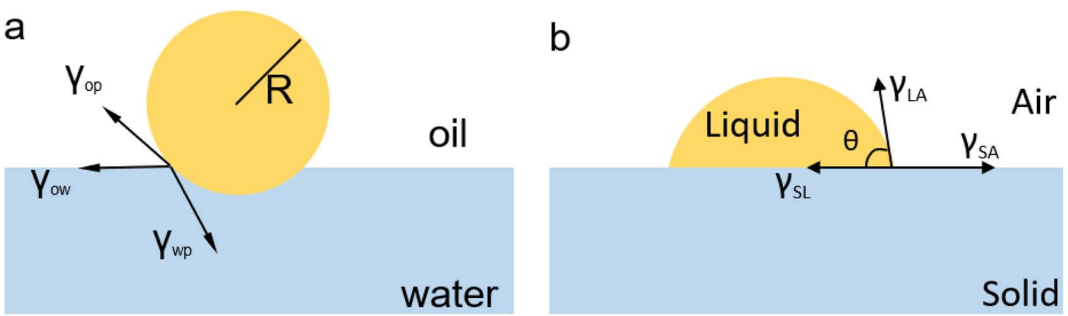

Fig. 1 (a) A schematic illustration of the interfacial absorbed NP, where R is the radius of NP. (b) Schematic illustration of a sessile droplet on a solid surface, with the relationship between the CA and surface tension γ. Reproduced with permission.[22] Copyright © 2019 Wiley-VCH GmbH.

nanoparticles and negatively charged ligands at the water–oil interface. The resulting nanoparticle-surfactants are strongly immobilized on the interface, forming densely packed assemblies at the liquid interface. This approach offers a way to prepare different liquid mixture systems, including ultra-stable Pickering emulsions, bi-jels, and structured liquids.[22,36,37] These fundamental studies on liquid interfaces built up the foundation for manipulating liquid interfaces for energy conversion and harvesting at liquid–liquid interfaces.

2.1.2. Liquid–solid interface. Not limited to the liquid–liquid interface, reactions at the liquid–solid interface are also crucial for the energy conversion from the nanoscale to the macroscale. Examples include catalytic reactions at the surface for nanosized catalysis and triboelectric applications on artificially designed surfaces.[38,39] When a liquid droplet is placed on a solid surface, the droplet will either remain sessile on the surface or wet the surface by spreading over it. The behavior of the liquid is determined by the surface energy. The formation of a unit area of the fresh solid–liquid interface will endow the interface with a certain amount of energy. If this energy is higher than that of a unit area of the newly formed liquid–air interface, the solid surface will be wetted by the liquid.[40] This process can be described in Fig. 1b in the following equation:

$$\cos\theta = (\gamma_{SA} - \gamma_{SL})/\gamma_{LA} \quad (4)$$

γ_{SA}, γ_{SL}, and γ_{LA} are the interfacial energy of the solid–air, solid–liquid, and liquid–air interface, respectively.

Surface modification can effectively alter the interaction between liquids and solids by modifying their structural morphology or chemistry. In a study reported by Jiang and colleagues,[41] surface engineering was used to create surface structural anisotropy, causing the spontaneous directional movement of liquid droplets by generating a surface energy gradient. The spindle-knot, as shown in Fig. 2a, was employed to achieve surface structural anisotropy along the fiber, forming a discontinuous three-phase contact line. Due to its higher hydrophilicity and apparent surface energy compared to the joint, the spindle-knot created a different CA on either side of

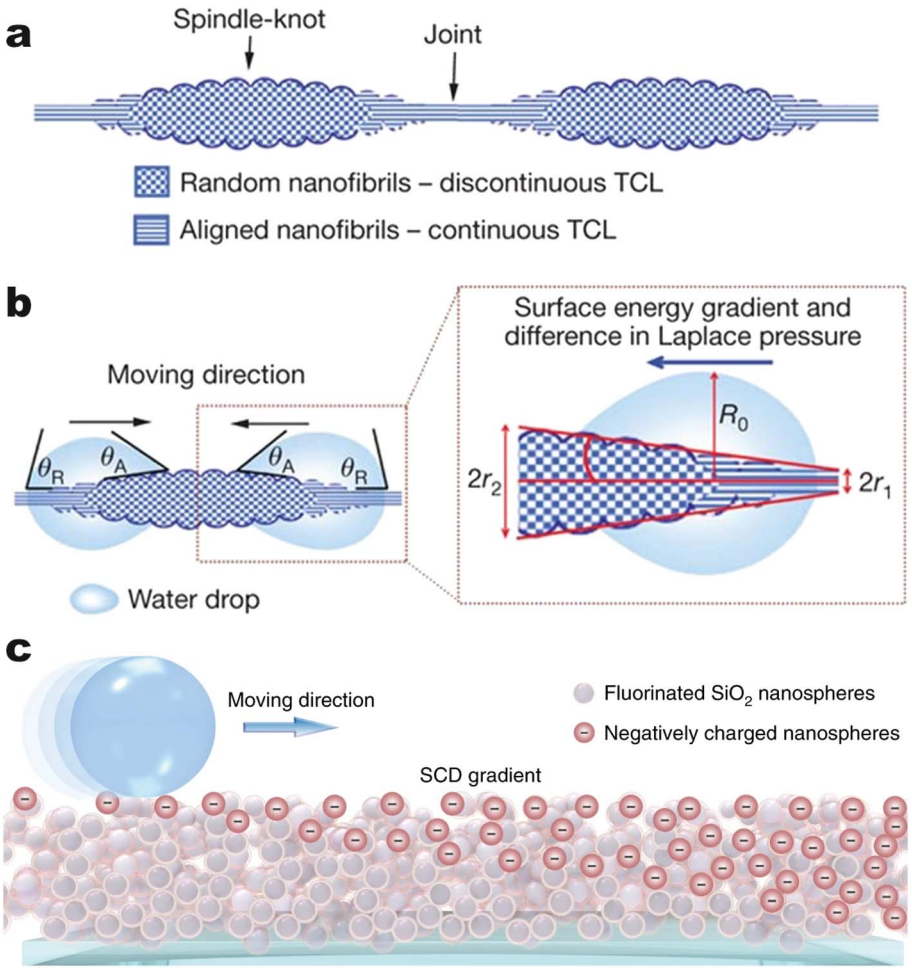

Fig. 2 (a) Spindle-knots are formed by randomly arranged nanofibrils, while joints between spindle-knots compose nanofibrils with well-distinguished ordered alignment. (b) Surface structural morphology variation induces a decay gradient of surface energy in the direction from spindle-knots to joints. The arrows denote the directions of drop movement. Reproduced with permission.[41] Copyright © 2010, Springer Nature Limited. (c) Illustration of droplet self-propulsion on a super amphiphobic surface decorated with a gradient distribution of charge density along with the surface. Reproduced with permission.[42] Copyright © 2019, Springer Nature Limited.

the droplet, resulting in a surface energy gradient and a variance in Laplace pressure. This pressure acted as the driving force for the directional movement of the droplet. Such a modification of the liquid–solid interface provides a convenient way for water collection in natural environments.

Surface chemistry modification can induce additional interfacial interactions between liquids and solids by changing the chemical potential of the interface. In a study by Sun *et al.*, self-propelled transport of droplets on a solid surface was achieved by modifying the surface *via* chemical vapor deposition (CVD), as shown in Fig. 2c.[42] When a droplet impacted on the solid surface, the impacting surface became charged, inducing charge density gradients on the liquid–solid interface. These gradients stimulated the directional self-propelling movement of the droplet, allowing for water harvesting.

2.2. Methods to manipulate the properties of the liquid interface

The properties of the pristine liquid interface are determined by the intricate nature of the liquid and/or solid interface. Therefore, it is crucial to develop controllable methods to manipulate the liquid interface according to various application needs. In the case of a liquid–liquid interface, extensive research has reported that the interface can be effectively manipulated by attaching interfacially active species such as surfactants, amphiphilic colloidal particles, polymers, and more.[29,43,44] On the other hand, for a solid–liquid interface, methods such as solid-surface chemical modification, surface etching, and the formation of self-assembled monolayers of functionalized colloidal particles have demonstrated their capability of manipulating the properties of the interface.[45–50] In this section, we will delve into the recent advancements in methods for modulating liquid–liquid and liquid–solid interfaces, respectively.

2.2.1. Interfacial assembly of nanomaterials at the liquid–liquid interface. Any interfacially active species has the ability to spontaneously assemble at a liquid–liquid interface, thereby altering interfacial properties such as interfacial tension. This review focuses specifically on the interfacial assembly of nanomaterials at the liquid interface and how these assemblies dictate the macroscopic behavior of liquid interfaces. NPs can assemble at the liquid interface, effectively reducing interfacial tension. If the energy consumed by desorbing a particle from the interface exceeds thermal fluctuations, this assembly process can be irreversible. Therefore, the accumulation of nanoparticles at the liquid interface leads to the formation of a dense colloidal layer, resulting in what is known as interfacial jamming. This jammed interfacial colloidal layer acts as an elastic coating, imparting solid-like stiffness to the liquid interface. Consider a water droplet immersed in oil. Without the interfacial assemblies, the droplet has a spherical shape as it has the smallest interfacial area, which is energetically favorable. However, with this interfacial colloidal coating, the liquid droplet retains a non-spherical shape because the solid-like interfacial layer can prevent the droplet from reducing its interfacial area. These interfacial-jammed liquids are called structured liquids, which were first proposed by Cui *et al.* in 2013.[33] Since then, the use of the interfacial assembly of nanomaterials has started to attract researchers' attention, and various applications have been proposed based on this simple yet powerful method, such as all-liquid 3D printing, all-liquid batteries, and all-liquid microreactors. In this section, we will overview the recent progresses in using different physical–chemical interactions to manipulate the liquid interface by means of interfacial jamming.

2.2.1.1 Electrostatic interactions. NPs with or without interfacial activity can assemble at the liquid interface to reduce interfacial tension. In this process, the interaction between NPs and the liquid interface dominates the method and path that NPs realize the assembly. Among various interactions, electrostatic interaction is the mostly studied and employed.[7,51,52] Various methods have been reported to adjust the interfacial assembly of NPs at the liquid interface by tuning the electrostatic interactions, which can be roughly categorized into two types: changing the pH value or ionic strength. The pH value is strongly associated with the pK_a of chargeable functional groups, such as $-COO^-$ and $-NH_3^+$. Huang *et al.* demonstrated that a higher pH (>5) can deprotonate –COOH into $-COO^-$, enhancing the interaction between PS-COOH and PDMS-NH_2.[53] Regarding the manipulation of ionic strength, Chai *et al.* elucidated the influence of ionic strength on the absorption of nanoparticles: higher ionic strength facilitates the interfacial absorption of NP-COOH and PDMS-NH_2, thus increasing the packing density of the area. The packing of NPs at the liquid interface can be finely controlled by varying the ionic strength.[54]

Using electrostatic interactions, NPs can assemble at the liquid interface and endow the interface with intriguing properties, such as response to external stimuli. External stimuli can trigger the controlled movement of single functionalized nanoparticles (NPs) at the liquid interface. As an example, Dietrich *et al.* assembled Janus colloids with an Au cap at water–oil interfaces and utilized laser light illumination to induce asymmetric heating.[55] In this process, temperature and surfactant concentration gradients were generated, inducing Marangoni stresses that transformed the NPs into microscale surfers. If the NPs become jammed at the liquid interface, the mobility of individual particles is restricted due to the dense packing of the particles. As a result, when external stimuli are applied to the jammed nanoparticles, the behavior of all NPs dominantly affects the interface through the synergetic effect.[56]

Cui *et al.* created nanoparticle surfactants *in situ* at the interface with carboxy-functionalized NPs from the water phase and amine-group functionalized polymers from the oil phase.[33] Electrostatic interactions not only dictate the arrangement of NPs but also cause different shear forces of the liquid phases. Fig. 3a and b show that an external electrical field reshaped a water droplet that was immersed in high-viscosity silicone oil. After reshaping, the water droplet exposed an additional fresh interface capable of accommodating more nanoparticle surfactants. The jammed nanoparticle surfactants then impeded the recovery of the shape and maintained an ellipsoid shape for more than a month.

Another accessible stimulus that can be used to trigger the responsive behavior of NPs is magnetic force. Liu *et al.* attempted to attach superparamagnetic Fe_3O_4 NPs to the water–oil interface, resulting in a ferromagnetic liquid droplet.[57] However, once the Fe_3O_4 NPs were trapped at the surface, the magnetism could not be removed unless the NPs were disassembled from the interface. Recently, Zhao *et al.* used Fe_3O_4 NPs as "hammers" to deform the liquid–liquid interface, while oleic acid and amine group functionalized silica NPs assembled and jammed the interface.[6] As shown in Fig. 3c and d, an external magnetic field deforms the liquid interface, and the nanoparticle surfactants lock the deformed interface through electrostatic interaction. When the external magnetic field is removed, the interface returns to its non-magnetic state.

2.2.1.2 Host–guest recognition induced interfacial assembly. Molecular recognition between host and guest molecules, based on non-covalent interactions, can be utilized to actively control the interfacial assembly of nanoparticles and ligands, thereby offering a method to manipulate liquid interfaces. This type of interaction involves a host unit acting as the receptor and a guest unit as the ligand. Various host units, including crown ethers,[58] cucurbit[*n*]uril,[59] cyclodextrins,[60] and calixarenes,[61] have been reported as receptors, providing a range of options to adapt to different conditions. In contrast to electrostatic interactions, which only respond to changes in pH, ionic strength, or temperature, host–guest pairs offer the potential to manipulate the liquid interface using a wider range of external stimuli by altering the assembly–disassembly of the host–guest pairs.

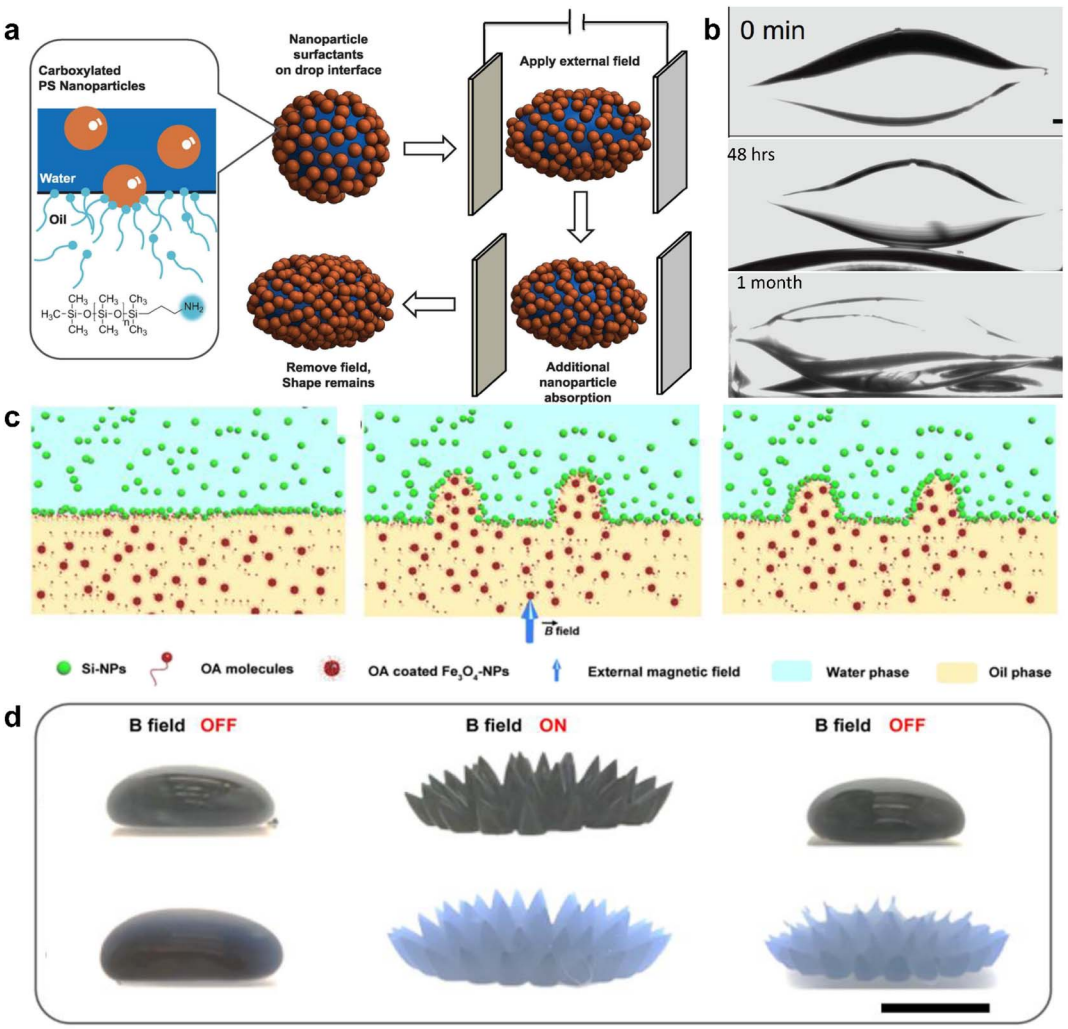

Fig. 3 (a) Schematic demonstration of shape evolution of a NPs clad droplet from a sphere to an ellipsoid when an electric field is applied. Even after the electrical field is removed, the deformation is maintained due to the interfacial assembly of NP surfactants. (b) A time-sequenced snapshot of the deformation process of a water droplet, in which 15 nm carboxylated polystyrene NPs are dispersed with 1 wt%, and the outer phase is silicone oil dissolved with PDMS-NH_2. The original spherical droplet has a diameter of 1.8 mm. Reproduced with permission.[33] Copyright © 2013 American Association for the Advancement of Science. (c) Schematic cartoon illustrating the deformation of the water–oil interface under a magnetic field and its maintenance after the field is removed. (d) Real pictures of the water–oil interface structured and locked by an external magnetic field. (Upper panel) Picture showing the FF droplet suspended in pure water. (Lower panel) Picture showing the FF droplet immersed in Si-NPs dispersion. Scale bar, 5 mm. Reproduced with permission.[6] Copyright © 2022 American Chemical Society.

Shi and colleagues have investigated the potential of host–guest molecular recognition for manipulating liquid interfaces. The non-covalent interaction between host and guest units forms supramolecular structures that assemble at the liquid interface, creating interfacial films with solid-like characteristics that can regulate mass transport across the interface. Sun *et al.* developed a pair of α-CD-functionalized Au NPs and azo-terminated poly(L-lactide) (Azo-PLLA) ligands that are responsive to photo illumination to create a structured liquid.[5] PLLA and water/α-CD interact with each other through hydrogen bonding, holding NPs and ligands at the interface, thus increasing the binding energy of NPs at the liquid interface and enabling the control of mass transport between the two phases. Upon UV irradiation, the *trans*-Azo-PLLA photoisomerizes to *cis*-Azo-PLLA, then the host–guest recognition works. In detail, *cis*-Azo-PLLA is pulled out of the pocket in α-CD. Finally, the binding energies of the nanoparticles surfactants (NPSs) will be deduced, and the assembled NPs will be restricted from the liquid interface, leading to the disassembly. Li *et al.* went a step further by using α-CD NPs/Azo-PLLA as a photoresponsive gate to regulate molecular diffusion at the liquid–liquid interface (Fig. 4a).[62] After 2D assembly formation, UV irradiation triggers a jamming-to-unjamming transition, releasing trapped Rhodamine B from the water phase into the oil phase. This photo-responsive gate can control molecular diffusion across the water–oil interface, regardless of the interface's shape (Fig. 4c–e), offering a promising approach to regulating heterogeneous reactions.

By utilizing different molecules, host–guest pairs can exhibit redox-triggered responses in addition to photo-responsiveness. Several pairs exhibit sensitivity to changes in redox conditions, such as Fc-terminated poly-L-lactide (Fc-PLLA)/β-CD,[63] naphthalene/methyl viologen,[64] Fc-PLLA/polyoxometalate,[65] and polystyrene with termination pillar[6]arene (PA[6])/ferrocenium (Fc^+-PS).[66] Reversible charge transfer occurs between the donors and acceptors. Thus, assembly–disassembly can be initiated accordingly. As illustrated in Fig. 4f, the uncharged Fc is bound tightly in the cavity of β-CD through host–guest recognition. As the redox process is carried out, the charged Fc^+ is generated and dissociates rapidly. Reversible jamming and unjamming states can be achieved, as shown in the pendent drop experiments (Fig. 4g). By now, various approaches have been developed to realize the manipulation of liquid–liquid interfaces, as summarized in Table 1. By different methods,

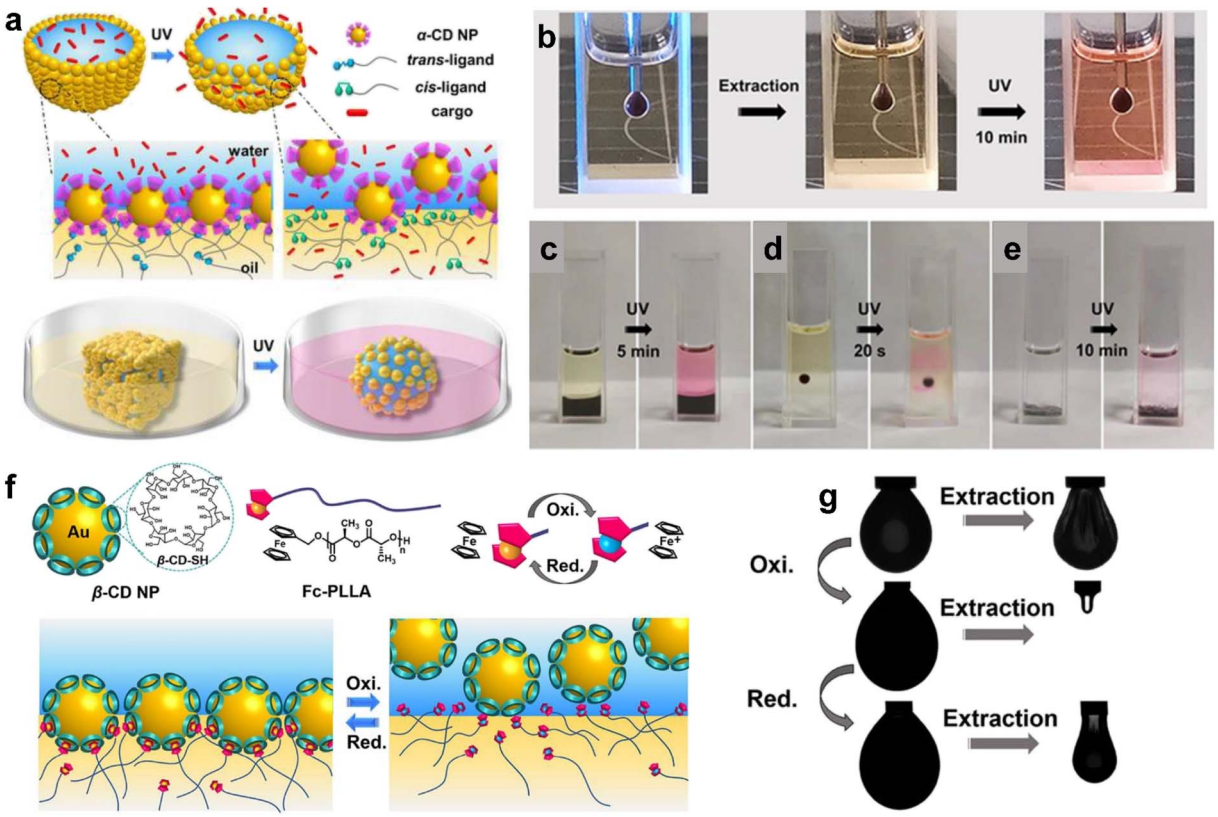

Fig. 4 (a) Cartoon illustration of photo-responsive droplets (top) and conversion of a droplet from cubic to spherical shape, controlled cargo release endorsed by interfacial jamming (bottom). (b) Optical image of (b) pendant droplet, (c) interfacial membrane, (d) single droplet, and (e) microcapsules demonstrate the jamming-controlled diffusion of Rhodamine B triggered by 365 nm UV light irradiation. [α-CD NP] = 1.0 mg mL^{-1}, [Azo-PLLA] = 1.0 mg mL^{-1}, [Rhodamine B] = 1.0 mg mL^{-1}. Reproduced with permission.[62] Copyright © 2021 Wiley-VCH GmbH. (f) Schematics of structures of the developed β-CD NP and Fc-PLLA (upper left) and the corresponding reduction and oxidation state of Fc (upper right). Schematic illustration showing the reversible assembly/disassembly process of s-NPSs at the oil–water interface in a UV light-induced redox process (bottom). (g) Reversible jammed and unjammed states switched by redox-switchable reconfiguration. Reproduced with permission.[63] Copyright © 2021 American Chemical Society.

Table 1 Typical NPs/ligands/polymer pairs and corresponding interactions[a]

Interaction	Liquid A	Liquid B	NP pair	Responsive condition	Ref.
Electrostatic interaction	Water (PEG)	Water (dextran)	PDADMAC & PSS	NA	67
	Silicone oil	Water	PDMS-NH_2 & PS-COOH	Electric field	33
	Mineral oil	Water	SiO_2–NH_2 & oleic acid, incorporated with Fe_3O_4 NPs	Magnetic field	6
	Toluene	Water	POSS-NH_2 & FPNPs	pH	68
	Toluene	Water	POSS-NH_2 & DNA	NA	69
	Toluene	Water	POSS-NH_2 & MXene	NA	70
Host–guest recognition	Toluene	Water	Fc-PLLA & PEI-β-CD	Electrochemical redox responsiveness	71
	Toluene	Water	PS-MV^{2+} & cucurbit[7]uril	Guest-competitive responsiveness	72
	Toluene	Water	Azo-PLLA & Au-NPs	Photo-responsive	5
Electrostatic interaction/hydrogen bonding	DMF	Octane	POSS-NH_2 & PHEMA-*g*-PAA	NA	73
Electrostatic interaction & intermolecular π–π stacking	Oil	Water	H_6TPPS & amine-terminated polymer/oligomer ligands	NA	74
Electrostatic interaction/hydrogen bonding	Silicone oil	DMSO	POSS-NH_2 & CNC	NA	75
Charge-transfer interactions	Toluene	Water	NT-terminated poly-L-lactic acid & MV^{2+}	Electrochemical redox responsiveness	64

Appendix of table 1: name of chemicals and corresponding abbreviations

Name	Abbra.
Poly(diallyldimethylammonium chloride)	PDADMAC
Poly(sodium 4-styrenesulfonate)	PSS
Amine-functionalized polyhedral oligomeric silsesquioxane	POSS-NH_2
Poly(2-hydroxyethyl methacrylate)-g-poly(acrylic acid)	PHEMA-*g*-PAA
Ferrocene (Fc)-terminated poly-L-lactide	(Fc-PLLA)
β-Cyclodextrin (β-CD)-modified branched polyethyleneimine	PEI-β-CD
Cellulose nanocrystal surfactants	CNC
Fluorescent polymeric nanoparticles	FPNPs
Methyl viologen-terminated polystyrene	(PS-MV^{2+})
5,10,15,20-Tetrakis(4-sulfonatophenyl)porphyrin	H_6TPPS
Azo-terminated poly-L-lactide	Azo-PLLA
α-CD-modified gold NPs	(Au-NPs)

[a] Note: "NA" means the system is not able to respond to external stimuli.

people can use suitable ways to control the properties of liquid–liquid interfaces.

2.2.2. Modification of the liquid–solid interface. Most energy conversion reactions occur on solid surfaces, particularly in the case of heterogeneous catalysis, water harvesting, desalination, and other related processes.[39,41,76] The wettability of the solid surface by liquids plays a crucial role in facilitating these reaction processes. Surface modifications, involving structural engineering and chemical modifications, are employed to enhance the interaction between the liquid and solid at the liquid–solid interface.

2.2.2.1 Structural morphology modification of the solid surface to alter the wettability. Reducing the surface energy and increasing the surface roughness are two key strategies to alter the wettability of liquid on a solid surface. Surface roughness gives rise to surface energy gradients, which can actuate the liquid droplet to relocate to the more wettable region with higher surface energy, as described by Wenzel's law:[77]

$$\cos\theta_w = r\cos\theta \quad (5)$$

where r represents surface roughness, θ_w is apparent and intrinsic CA on rough surfaces, and θ represents intrinsic CA of liquid on smooth surfaces. In Fig. 5a and b, Zhang *et al.* reported a V-shaped prism microarray (VPM) surface fabricated by photo-etching and a subsequent dip coating process.[78] As the V-shaped array is fabricated from temperature-responsive Poly(*N*-isopropylacrylamide) (PNIPAAm), intermolecular or intramolecular formats reversibly, which contributes to the reversible swelling upon changing the temperature below and above the lower critical solution temperature (LCST). By regulating the apparent roughness of the surface, the V-shaped array affords a reversible transition of θ_w between 107° and 25° (Fig. 5c and d), contributing to the switchable wetting behavior and directional movement of liquid droplets over the solid surface.

To improve the lyophilicity and lyophobicity of surfaces, researchers have been exploring nature-inspired structures,

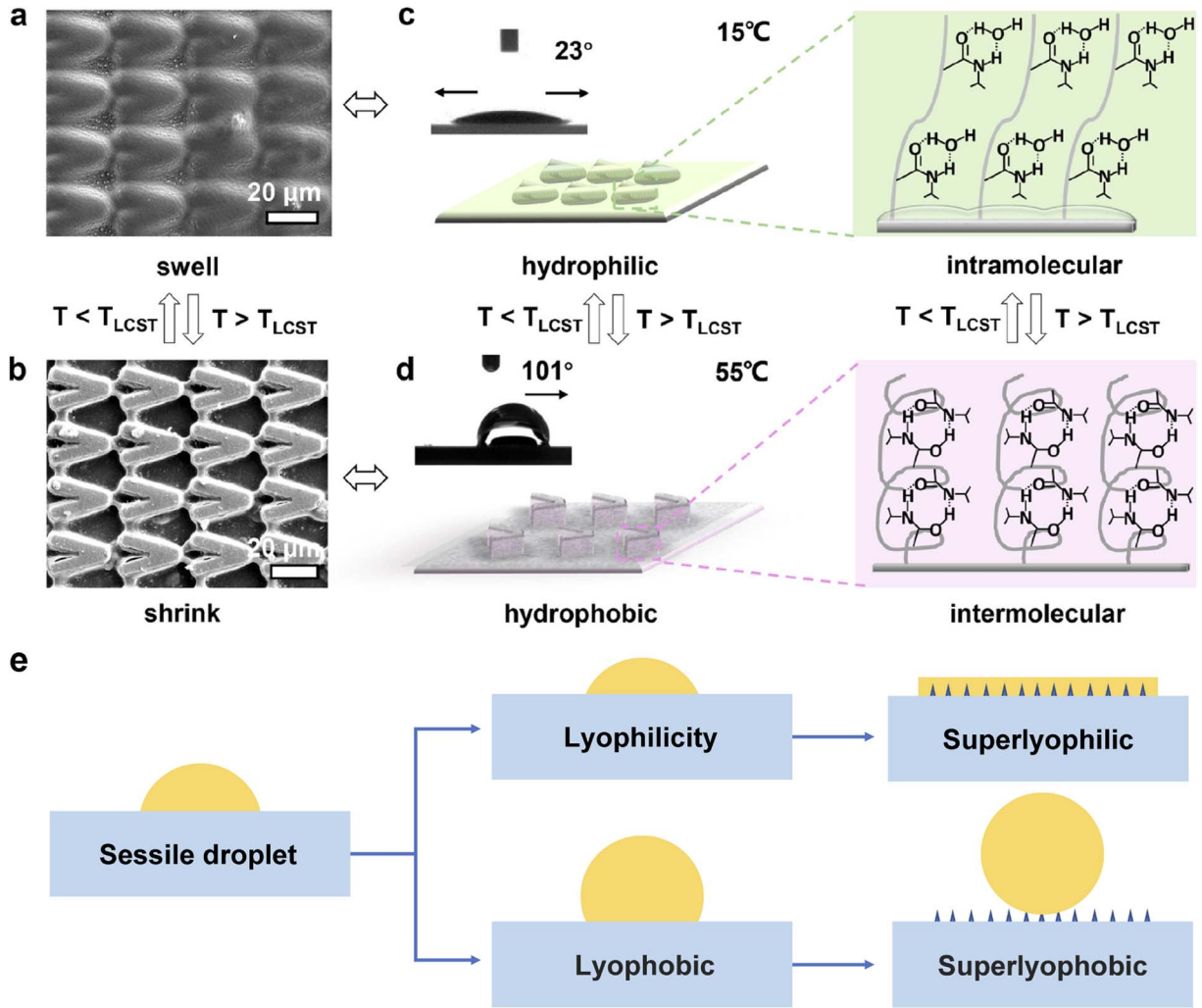

Fig. 5 (a and b) Scanning electron microscopy image of the temperature-responsive (PMMA/PNIPAAm/TiO_2-coated) VPM surface with parallel micro/nanostructure ($\phi = 30°$): controllable swelling and shrinking of the patterns by manipulating temperature. (c and d) Schematic diagrams and CA photographs of the surface corresponding to (a) and (b), showing that the surface properties related to the surface structure, *i.e.*, hydrophilicity with bidirectional wetting below LCST and hydrophobicity with orientated wettability along +*x* direction above LCST. Reproduced with permission.[78] Copyright © 2020 American Chemical Society. (e) Roughness influences the properties of the surface: lyophilic and lyophobic. Adapted with permission.[79] Copyright © 2017 Springer Nature.

including lotus leaves,[80] fish scales,[81] salvinia,[3,82] *etc.* Lotus leaves have a unique rough morphology with a papilla structure, resulting in a difference between the apparent and intrinsic CAs of liquid on the surface.[80] By incorporating appropriate multi-scale structures on solid surfaces, the wetting state can be enhanced from lyophilicity to superoleophilicity, as shown in Fig. 5e. To achieve the appropriate nano/micro-structure of the solid interface, interfacial materials with various dimensionalities are being investigated, such as incorporating 0D particles, 1D fibers, and channels onto the solid surface. Moreover, if the attached particles or fibers are decorated with specific species, the functionality of the solid surface can be widely adapted.

Besides altering surface roughness, the surface energy on a solid surface can be altered by employing specific materials, such as TiO_2, whose surface energy/wettability can be tuned by changing the light illumination. As reported by Wang *et al.*, a TiO_2-coated glass can demonstrate a highly amphiphilic nature, which can be ascribed to the coexistence of hydrophilic and oleophilic areas on the surface of the TiO_2 coating.[83] In detail, the UV-irradiation induced the emergence of oxygen vacancies, resulting in the adsorption of dissociative water. Similarly, Shen *et al.* report on potential-regulated hydrophobicity/hydrophilicity at cobalt-based oxide interfaces with an alkaline solution.[84]

2.2.2.2 Chemical modification to tailor the interaction between liquid and solid surfaces. The degree of wetting between a liquid and a solid surface is primarily influenced by the chemical composition of both surfaces. Thus, chemical modification of the solid surface (*e.g.*, coating/grafting, polymerization, redox reactions, and CVD) provides a viable approach to controlling the interaction between the liquid and the solid.

For instance, the functionalization of graphene to graphene oxide (GO) introduces numerous surface functional groups, including –OH and –COOH, which enhance its hydrophilicity.

Incorporating GO as a building block in the design of solar steam generation devices facilitates water absorption, transportation, and evaporation, thereby improving the efficiency of desalination processes.[85] Then, chemical grafting of alkylamine on the surface of GO can realize the modification of GO and result in the amphiphilic Janus nanosheet.[86] Besides grafting to the surface, monomers can also directly polymerize on the surface to form a thin layer, which in return modifies the wettability of the solid surface. Song *et al.* polymerized two hydrophobic monomers, butyl acrylate (BA) and 2-ethylhexyl acrylate (2-EHA), on cellulose fibers to transfer the hydrophilic surface to be hydrophobic, indicated by the increased CA from 0° to above 127°.[87] In addition, chemical reactions, such as redox reactions, are also used as an efficient strategy to modulate the wettability of the solid surface. Li and co-workers reported a feasible way to realize the reversible hydrophobic to hydrophilic transition in graphene *via* water splitting.[88] Upon UV irradiation, H_2O molecules are split into hydrogen and hydroxyl radicals, thus promoting the dissociative adsorption of H_2O molecules. Then a wettability transition from hydrophobicity to hydrophilicity can be realized, as indicated by the reduced CA from 97.7° of untreated graphene to 39.2° for UV-treated graphene.

Chemical modification serves not only to change the interfacial tension but also to generate additional interactions between the liquid and solid surfaces. When two materials make contact, contact electrification takes place at the interface, which includes the effects observed when a liquid droplet impacts a solid surface. It is essential to chemically modify the solid interface in order to leverage this reaction for controlling the liquid interface or the movement of liquid droplets.[89] Sun *et al.* developed a superamphiphobic surface by coating a glass substrate with an approximately 10 μm-thick nanoporous SiO_2 layer and a hydrophobic layer of 1H,1H,2H,2H perfluorooctyltrichlorosilane (PFOTS), which is prepared by CVD, as shown in Fig. 2c.[42] Upon impact, the droplet spreads, retracts, and rebounds from the surface, as well as becomes charged on the impacted surface, as illustrated by Fig. 6a. By configuring the solid surface with a surface charge gradient, the charged liquid droplet will be driven by the electrostatic force in

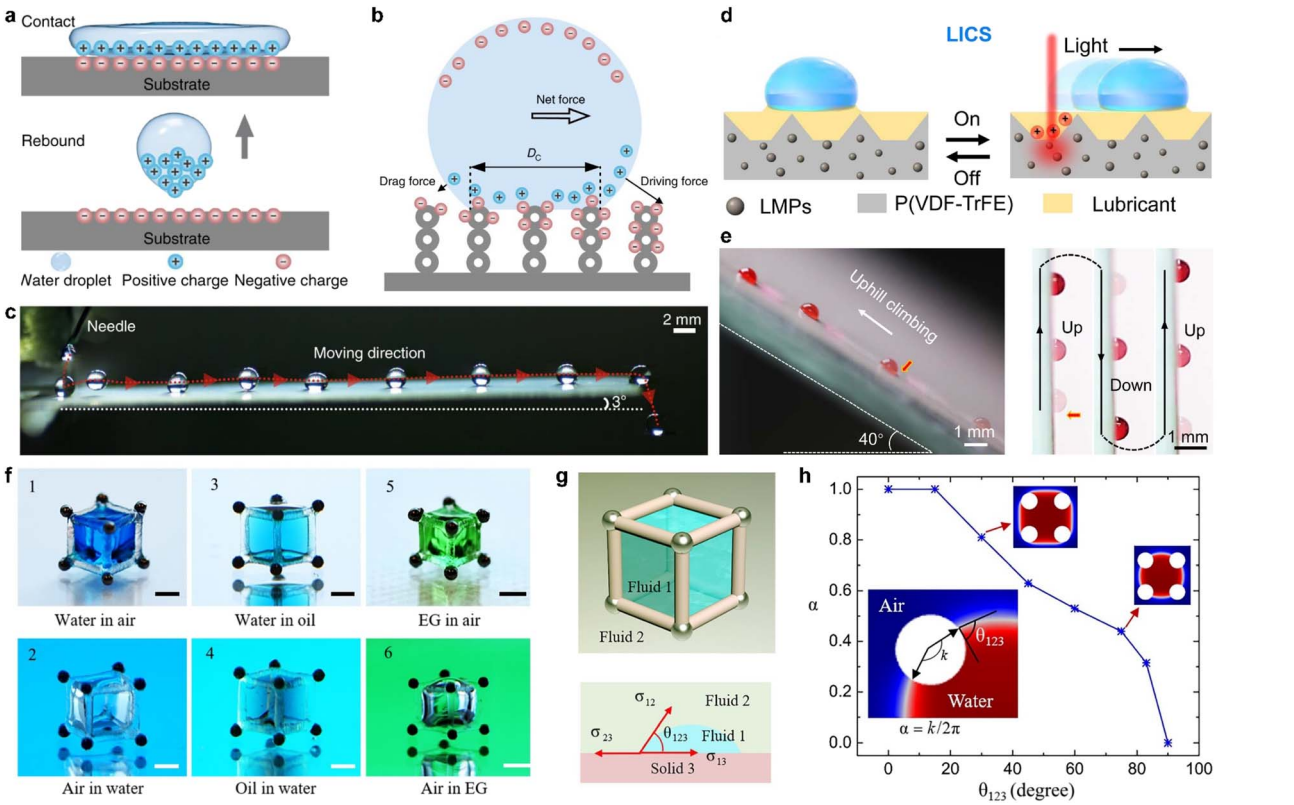

Fig. 6 (a) A cartoon diagram illustrating the charging process of a superamphiphobic surface during the droplet impacting process. (b) A schematic of the droplet transport mechanism. Due to the SCD gradient, an unbalanced electric force is induced and results in self-propulsion. (c) Picture shows the route of a moving water droplet in time-sequence on a superamphiphobic surface, featuring a SCD gradient modification and a 3° tilt. Reproduced with permission.[42] Copyright © 2019 Springer Nature. (d) Schematic illustration of the LICS for droplet manipulation. (e) (Left) The route of a moving water droplet in a time-sequence as it climbs upwards on a LICS while subjected to near-infrared irradiation. (Right) Pictures of the antigravity movement of a water droplet in a time-sequence on a vertically placed LICS. Reproduced with permission.[92] Copyright © 2022 American Association for the Advancement of Science. (f) Pictures of the six different immiscible fluid interfaces, marked from 1 to 6. Scale bars, 1 mm. (g) Schematic illustration of parameters of CA (θ_{123}) for the description of the capillary container. (h) Relationship between the wettability coefficient α and CA (θ_{123}) for water in the air. Reproduced with permission.[93] Copyright © 2021 American Association for the Advancement of Science.

a preferred direction (Fig. 6b and c). Increasing the surface charge gradient enhances the driving force, enabling the liquid droplet to climb from the bottom upwards without the need for additional energy input. Surface chemistry modification is extensively employed to manipulate the interaction between liquids and solids, which plays a critical role in harvesting water kinetic energy and offers novel insights into energy conversion and collection.[90,91]

The manipulation of liquid droplets on solid surfaces can be improved by incorporating external stimuli to achieve remotely controlled manipulation. Wang and colleagues developed a light-induced charged slippery surface (LICS), which involves constructing a composite matrix that is photothermal-responsive with real-time light-induced surface charge regeneration capability.[92] The LICS comprises Ga–In liquid metal particles that convert absorbed light into local heat and a hydrophobized silica nanoparticle (SiO_2 NP) layer for lubricant trapping. When illuminated with near-infrared (NIR) light, the LICS surface becomes positively charged, triggering droplet motion with a high speed of $\sim$18.5 mm s^{-1} and a long distance ($\sim$100 mm), as illustrated in Fig. 6d. The strong electrostatic interaction enables antigravity motion of the droplet with high spatiotemporal resolution, as demonstrated in Fig. 6e and f.

Chemical modification of solid surfaces provides a means to control the interaction between liquids and solid surfaces, including the transfer and redistribution of charges. This opens up opportunities to manipulate the movement of liquids on solid interfaces. It has been demonstrated that the motion of liquids is an energy conversion process, as seen in the antigravity motion induced by SCD gradients, which results in an increase in the potential energy of the liquid droplet.[42] Additionally, the controlled motion of liquids enables efficient water collection, which is crucial in water desalination techniques. Although the controllable motion of liquids through surface modification is still in its early stages, it holds great promise for energy conversion and harvesting applications.

2.2.2.3 Capillary force. Capillary force significantly influences the behavior and wetting state of liquids within confined spaces. It acts in balance with gravity and surface tension. By manipulating the interplay between these forces, somewhat "counterintuitive" phenomena in water movement can be observed. To actively control the movement of liquid, researchers have utilized a "capillary container" to confine the liquid within specific boundaries.[93] Song and colleagues achieved 3D architecture by using capillary forces for controllable dynamic modulation of liquid by trapping it in a magnetic-actuated capillary container, as shown in Fig. 6f. They elucidated the conditions for capillary trapping by building the system shown in Fig. 6g, where fluid 1 is confined in the capillary container in immiscible fluid 2, thus creating a structured 3D fluid. The wettability coefficient α is induced to describe the capillary trapping, which is dependent on the CA θ_{123} of fluid 1 on the skeleton (solid 3) in fluid 2. This determines the conditions for liquid trapping for water in the air, and by using this universal approach, various liquids can be trapped in specific magnetic-responsive capillary containers that can be used in different reaction systems. A simplified magnetic robot model consisting of two steel beads and a magnetic control system was developed to realize liquid transportation and mixing.[94] The magnetic robot can be easily controlled by an external magnetic field.

Capillary force alone can drive the self-propulsion of liquid without the need for any external stimuli. Feng *et al.* discovered a dual-reentrant surface with an asymmetric profile that allows fluids to spread out at both the surface and subsurface layers.[95] This design was inspired by the structure of the Araucaria leaf, which possesses ratchets arranged periodically and tilted towards the leaf tip. This unconventional yet effective approach to manipulating liquid has enabled the researchers to achieve 3D capillary containers for controllable liquid directional navigation.

3. Application of liquid interfaces in energy conversion

Liquid interfaces, including the liquid–liquid and liquid–solid interfaces, play a crucial role in various interfacial interactions, such as heterogeneous catalysis, water kinetic energy harvesting, water harvesting, and electricity generation. Modifying these interfaces can facilitate or finely control reactions, leading to improved energy conversion or harvesting efficiency, and the desired reaction path. Note that many catalysis reactions happen at liquid interfaces, especially liquid–catalysis interfaces. Herein, understanding the liquid interface is crucial for realizing the high-efficiency of catalysis and desired functions, such as selectivity and controllable reactions. In this section, we will discuss the recent advancements in the field of liquid interfaces and their applications in energy conversion and harvesting processes.

3.1. Interfacial assembly contributed reactors

Emulsions are of great importance in catalytic reactions for both industrial production and academic research. By emulsifying the reaction system, it is possible to create nano- or micro-sized emulsion droplets, which enhance the contact between the liquid phases and facilitate the distribution of the catalyst. This leads to improved catalytic efficiency.[96,97] Furthermore, the selective functionalization of the interface provides additional benefits for controlled reactions. By utilizing external stimuli-responsive interfacial assembly, it becomes feasible to achieve controllable macroscopic assembly of liquid droplets. This enables the selective triggering of reactions and offers greater control over the catalytic process.[96]

Xie *et al.* assembled hydrophilic Fe_3O_4 NPs and hydrophobic (TiO_2) NPs at a liquid interface and obtained Pickering emulsion microreactors, which integrated the magnetic and light responsiveness.[98] Different reactants are encapsulated in droplets in advance.[99] When applying an external stimulus, the droplets can be motivated towards each other by an external magnetic field, and a subsequent chemical reaction is initiated by UV irradiation, and the subsequent droplets coalescence and reactants mix. Taking advantage of the interfacial assembly, the size of the emulsion droplets can be tuned from 400 to 100 μm by simply changing the NP contents. The manipulation of the

position, movement, size, and coalescence of the emulsion droplets, enabled by the dual-responsive interface, is promising in controlling the chemical reactions inside the Pickering emulsion microreactors.

Yang *et al.* made use of multi-responsive surfactants based on functionalized nanoparticle dimers to manipulate, transport, and assemble liquid droplets and trigger the mass exchange and reaction.[99] As shown in Fig. 7a, gold (Au) nanoparticles are decorated with 11-mercaptoundecanoic acid (MUA), which has a –COOH termination, while Fe_3O_4 or PbS nanoparticles are modified with oleic acid (OA). These functionalized nanoparticles assemble and jam the liquid interface, forming a solid-like layer at the interface. For droplets stabilized by MUA-Au/Fe_3O_4-OA, the assembly of droplets can be initiated using a diode laser, and the macroscopic assembly/disassembly process can be repeatedly triggered with a light source (Fig. 7b). Furthermore, the use of an electric field can redistribute the assembled nanoparticles, creating a bare interface that allows two individual droplets to coalesce upon contact. This enables reagent exchange between the droplets. The presence of Fe_3O_4-OA enables droplet manipulation under the influence of a magnetic field. As depicted in Fig. 7d,

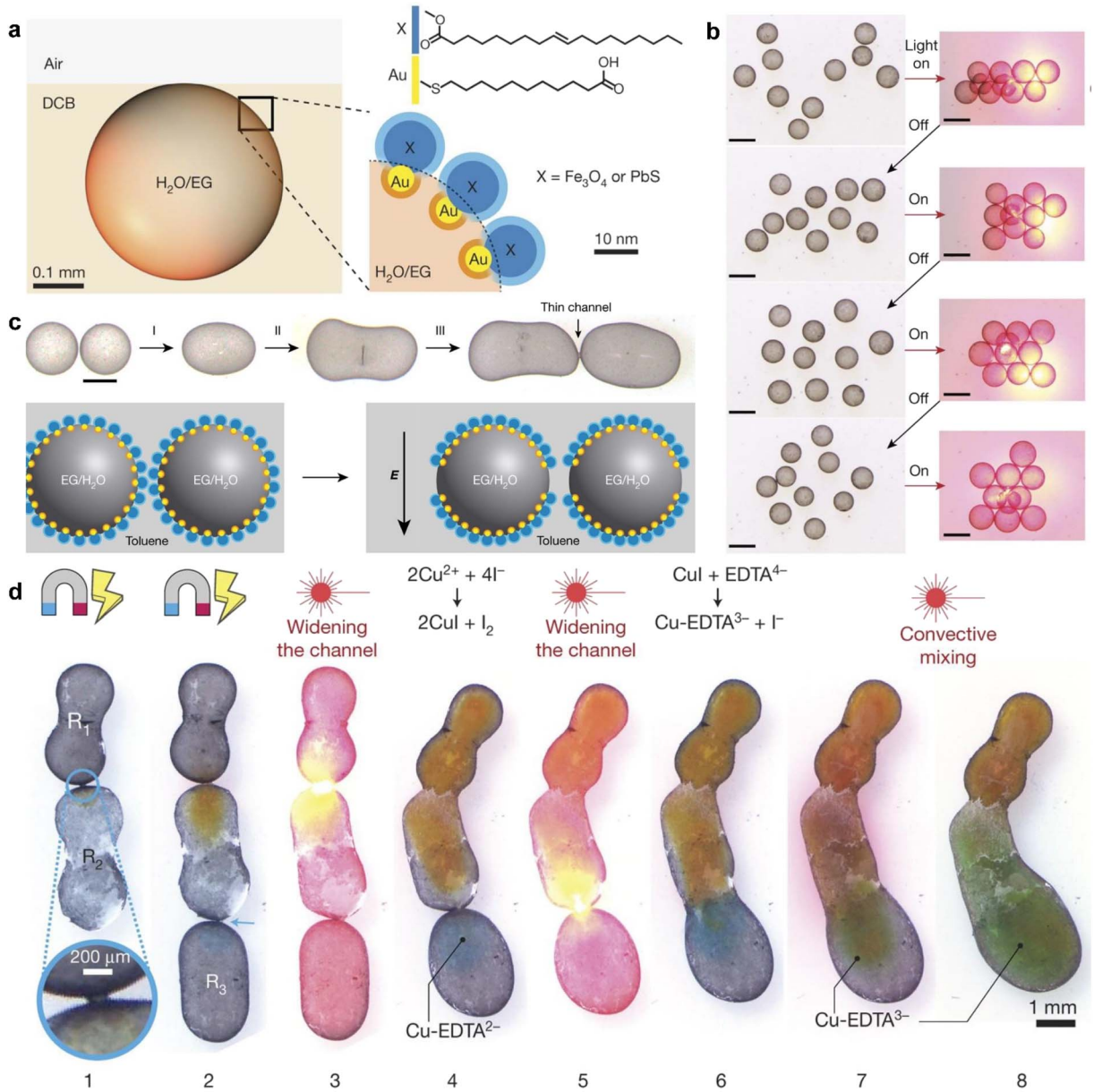

Fig. 7 Demonstration of multifunctional droplets, stablized by the assembly of NP surfactant and their interactions. (a) Water droplet containing ethylene glycol coated with MUA–Au/X–OA surfactants and suspended near the 1,2-DCB–air interface. (b) Light-controlled assembly–disassembly of droplets with radii *ca.* 900 μm into various different structures. The left column shows the optical pictures, while the right column shows schematics. Scale bars, 1 mm. (c) (Top) The process of droplet welding. Scale bar, 0.5 mm. (Bottom) Schematic illustration of the mechanism of droplet welding. (d) The droplet welding and reaction. Reproduced with permission.[99] Copyright © 2018 Springer Nature.

magnetic fields can control the orientation and coalescence of the droplets, facilitating mass exchange. This system combining the controllable assembly offers a promising way to control the liquid phase interactions by using the droplets as reactors.

3.2. Interface promoted catalysis and energy storage

Biphasic reactions are commonly used in organic chemistry to isolate sensitive products and protect them from side reactions and interfering by-products. Liquid interface assembly has shown promise in controlling chemical reactions by manipulating the liquid interface, facilitating mass transportation between different phases, and initiating chemical reactions through the functionalization of the interface with different functional nanoparticles. However, incorporating additional nanoparticles can result in side reactions, and ensuring the proper phase of catalysts can be challenging. To simplify the reaction system, one alternative is to incorporate catalytic functions into nanomaterials with interfacial activity, allowing catalysis to directly facilitate chemical reactions at the liquid interface between two phases. As the liquid interface is at the nanoscale, contact between reactants and catalysts is promoted, contributing to highly efficient reactions.

Crossley *et al.* developed a series of amphiphilic solid catalysts by combining hydrophobic nanotubes with hydrophilic oxides.[100] These amphiphilic solid catalysts can stabilize water–oil emulsions and catalyze reactions at the liquid–liquid interface. The liquid–liquid interface not only offers reaction sites but also enables precise control of the reaction due to its nanoscale spatial confinement. Recently, Zou *et al.* proposed a liquid–liquid interfacial effect to modulate the selectivity of hydrogenation catalyzation reactions at the Pickering emulsion interface.[101] As shown in Fig. 8a, Pt nanoparticles are deposited on the hydrophilic face of Janus mesoporous silica nanosheets and thus face the oil phase in the Pickering emulsion system. This allows precise control of the spatial distribution of catalysis at the water–oil interface. Regarding the hydrogenation of halonitrobenzenes, the reaction selectivity on the inner surface (up to 99.6%) is much higher than that in the outer interfacial layer (63.6%) and in other solvents (46.8–68.5%). The nanoscale microenvironments formed near the liquid–liquid interface are found to be crucial for high catalytic selectivity. Experimental and theoretical simulation results indicate that the direct contact of C–Cl bonds with the metal surface is restricted by modulating the absorption of reactants and products on the metal NPs, which are attached in the inner interfacial layer. This liquid–liquid interface-promoted reaction selectivity is highly dependent on the amphiphilicity of the catalyst, which stabilizes the interface and separates the products from reactants. This methodology is promising in interfacial catalysis and can employ a variety of Janus nanoparticles/sheets, such as amphiphilic graphene.

Microenvironments at the liquid interface can enhance catalysis, but they can also lead to nonequilibrium in chemical systems by sequestering reactive species, making it difficult to manage the amount of chemical energy stored in the system. To address this issue, Yan *et al.* proposed a solution by creating structured-liquid batteries (Fig. 8b and c).[102] In this system,

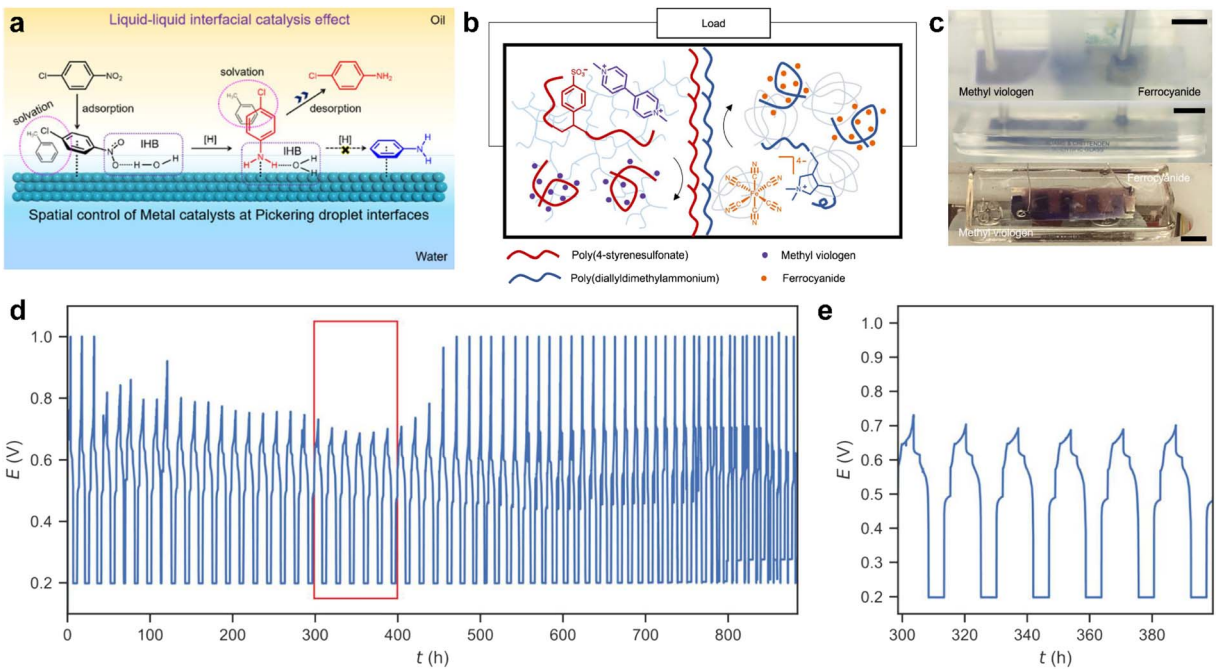

Fig. 8 (a) Schematic diagram of the reaction selectivity of *p*-CNB hydrogenation on the surfaces of Pd NPs, which is attached in the inner interface of Pickering droplets. IHB is referred to as the interfacial hydrogen-bonding interaction. Reproduced with permission.[101] Copyright © 2023 American Chemical Society. (b) Mechanism of all liquid batteries based on structured-liquid. (c) Real picture of the all-liquid battery based on the biphasic system in cycling. Scale bars: 1 cm. (d) Full cell charge/discharge curves with long-term cycles for an under-oil all-liquid battery. (e) Cycles from 20th to 25th (marked by the red box in (d)). Reproduced with permission.[102] Copyright © 2022 American Chemical Society.

polyelectrolytes are assembled at the interface to form an ionically permeable coacervate membrane between the anolyte and catholyte. Specifically, polyanions such as poly(sodium 4-styrenesulfonate) (PSS-Na) in the anolyte combine with polycations such as poly(diallyldimethylammonium chloride) (PDADMA-Cl) in the catholyte. This structure allows for precise control of the system and steady, rechargeable performance over hundreds of hours, as shown in Fig. 8d.

3.3. Electric generators

In 2014, Guo *et al.* put forward the concept of the "hydrovoltaic effect", which involves using the movement of ionized liquid over a solid surface to generate electricity.[12,103] They found that a few millivolts of voltage could be induced by moving a droplet of ionic solution (0.6 M NaCl aqueous solution) along a strip of graphene, as illustrated in Fig. 9a and b. The voltage is sensitive to the movement of the liquid, but a slight delay is detected, which is attributed to CA hysteresis. According to density functional theory simulations, hydrated Na^+ ions absorb on the surface of graphene with an adsorption energy of over 2 eV. On the contrary, hydrated Cl^- anions are repulsive to the surface of graphene. In this system, the adsorbed hydrated sodium cations lead to an accumulation of electrons, forming a pseudocapacitor, as shown in Fig. 9c–e.

The interaction between droplets and liquid or solid surfaces can lead to charge redistribution, resulting in the conversion of the kinetic energy of the droplet into electricity. This phenomenon has recently led to the development of droplet-based electricity generators, which hold great promise for energy harvesting.[42,91,104–107] When a droplet makes contact with a surface, the electrical double layer at the interface creates various interfacial charges, depending on the wettability of the liquid on the surface of the solid. Deng and colleagues demonstrated that the impact of a droplet on a superamphiphilic surface generates contact electrification and drives droplet movement.[42] Based on this, Xu and co-workers harvested the generated charges using polytetrafluoroethylene (PTFE), an electret material with high charge-storage capacity and stability.[91] Coupling PTFE with indium tin oxide (ITO) induces opposite charges of the same amount on the ITO, forming a charge storage system (Fig. 10a). The time-related increment of tested surface charges distribution on the PTFE film is shown in Fig. 10b, with a plateau obtained after the charging being saturated. Notably, the output voltage and current can reach as high as 143.5 V and 270.0 μA, respectively, delivering a rapid power density with peak value of 50.1 W m^{-2}. The system can light up 100 commercial LED diodes, demonstrating its potential application (Fig. 10c).

In addition to contact electrification, the piezoelectric effect can be harnessed in droplet-based electricity generators. Xu *et al.* demonstrated the use of a leaf-mimic rain energy harvester (REH) that enables the simultaneous harvesting of electrostatic and kinetic energy through the integrated effect of liquid–solid contact electrification and piezoelectricity.[107] The device consists of two parts: a transistor-inspired liquid–solid generator (TLG) positioned on the top and a piezoelectric energy harvester (PEH) located at the bottom (Fig. 10d and e).

When a droplet impacts the surface, the PEH promptly responds to the impact, generating a damping output that lasts for an extended duration. Simultaneously, a capacitor CE_2 is

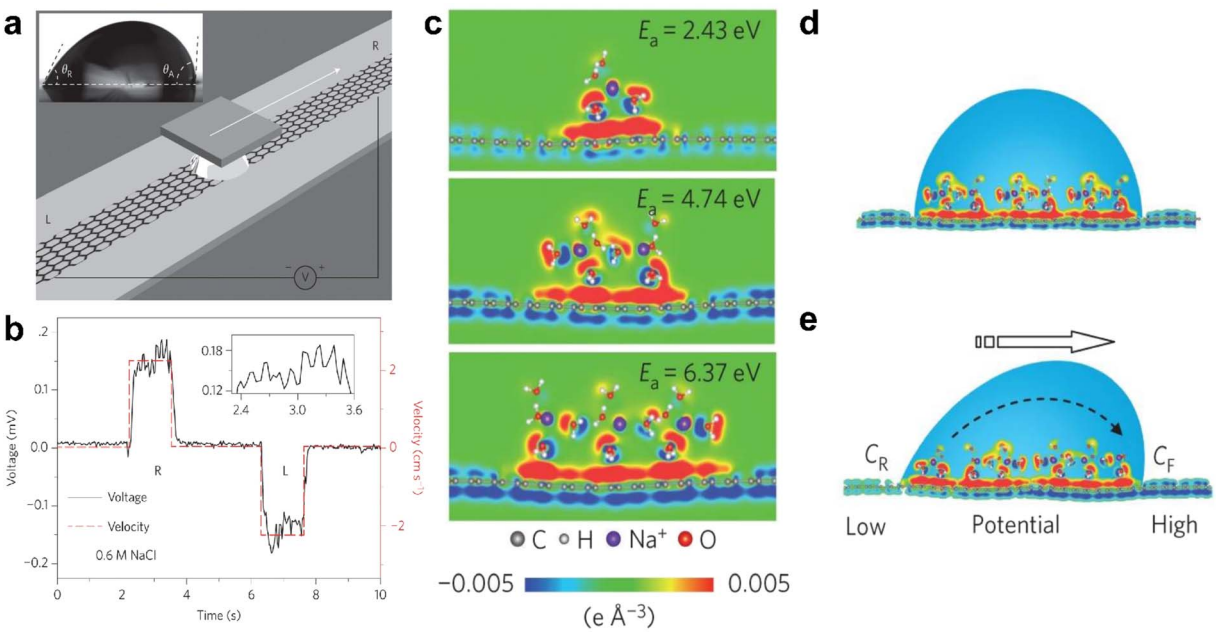

Fig. 9 (a) Schematic illustration of the droplet motion on the surface of graphene. (b) Typical voltage signal *versus* time when forcing the droplet to slip reversibly in between the left (L) and right (R) end of the graphene strip. (c) The distribution of differential charge near monolayer graphene at the different adsorption energies (E_a). (d and e) Schematic illustration of the pseudocapacitance formed by a static droplet on graphene and the difference in potential generated by the motion of the droplet on the surface of graphene. Reproduced with permission.[12] Copyright © 2014 Springer Nature.

formed at the water/copper interface, as illustrated in Fig. 10e. This setup allows for the collection of both the kinetic energy from the droplet impact and the electrostatic energy generated through contact electrification.

By combining the piezoelectric effect with droplet-based electricity generation, the leaf-mimic rain energy harvester offers a novel approach to harnessing energy from rainwater, leveraging both the mechanical impact and the electrostatic charge generated at the liquid–solid interface.[107]

Contact electrification, which typically occurs at the liquid–solid interface, can also be utilized to create energy-harvesting devices. Interestingly, it is also possible to build a similar system at the liquid–liquid interface. Wang and colleagues demonstrated the use of a liquid membrane as a permeable electrode to establish contact with liquid droplets, effectively acting as triboelectric nanogenerators (Fig. 11a).[106] To prepare the liquid membrane, a frame is employed to load a water/surfactant mixture. When the droplet falls, positive charges are generated on the droplet. The droplet then passes through the liquid film, and due to the existence of a grounded frame, electrons injection from the ground happens to neutralize the positive charges attached by the droplet. As a result, an electrical current can be generated once the circuit is closed. The dependence of the generated voltage and current on the volume of droplets is shown in Fig. 11b. The increment in both voltage and current with increased volume can be attributed to the enlarged surface area and the resultant more adequate friction between water droplets and air.

It is fascinating that the motion of droplets can generate electricity through triboelectricity, which can then be used to facilitate the continuous transportation of droplets.[108] This effect is known as the triboelectric wetting effect, which involves adjusting the wettability by introducing a non-uniform distribution of triboelectric charges. As illustrated in Fig. 10d, a grounded droplet on the floating potential (FP) surface is coupled with a positively charged virtual electrode. Increasing the surface charge density reduces the CA of a water droplet from 121° to 100° (Fig. 11e). When a conductive object comes into contact with and slides over the surface of the electrode in Fig. 11d, the virtual electrode is triboelectrified, affording the

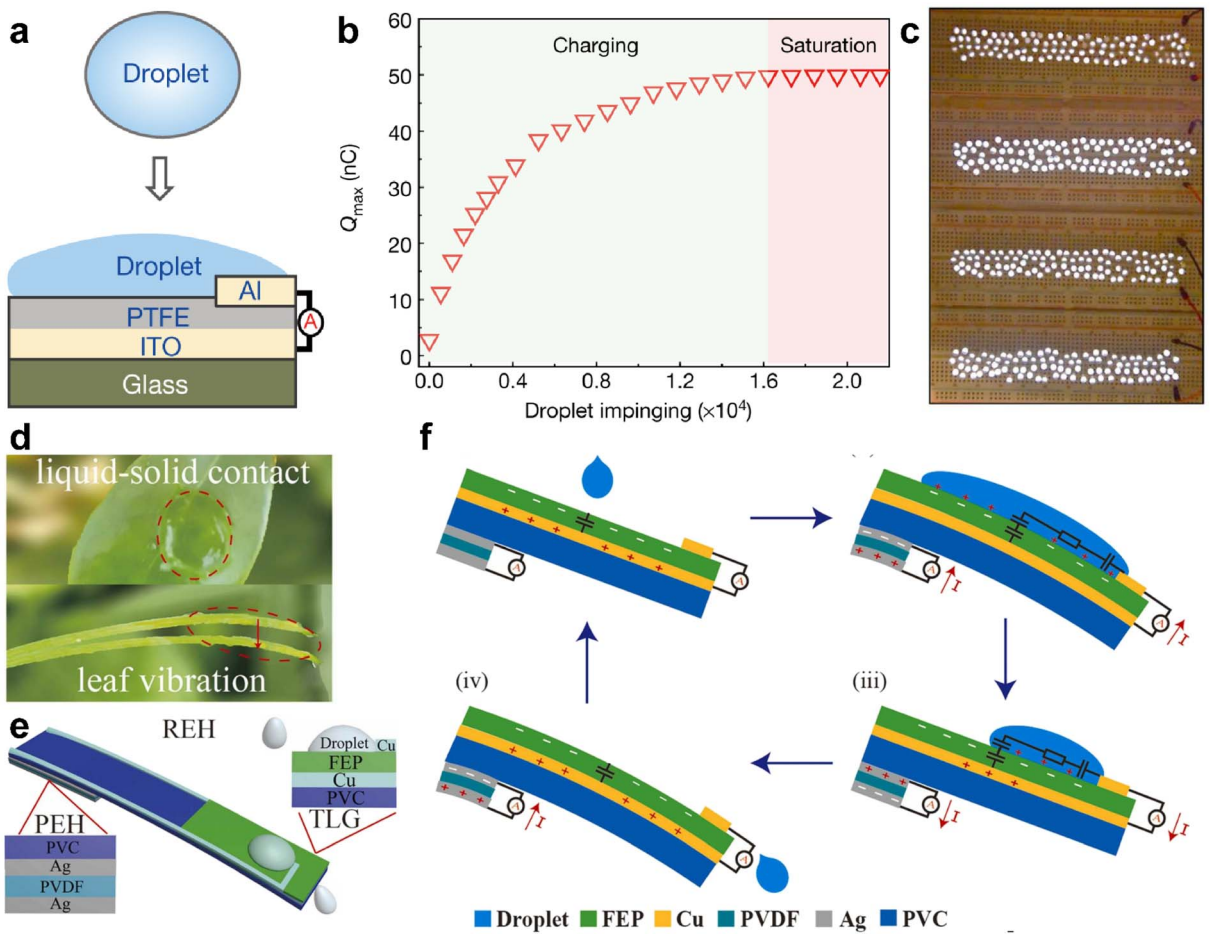

Fig. 10 (a) Schematic illustration of the layer-by-layer structure of droplet-based electricity generator (DEG) devices. (b) The charge accumulation on the PTFE surface with continuous impinge of the droplet onto the surface of DEG. (c) A demo showing that one hundred commercial LEDs can be lit up by the power generated by one droplet, and the height difference from the start point to the device is 15.0 cm. Reproduced with permission.[91] Copyright © 2020 Springer Nature. (d) Picture shows the impact of a droplet onto a leaf and the resulting vibration; (e) diagram showing the structures of the REH, integrating both liquid–solid contact electrification and the piezoelectric effect. (f) The working mechanism of the REH. Reproduced with permission.[107] Copyright © 2021 Elsevier.

driving force required for the motion of the top droplet (Fig. 11f).

3.4. Interfacial materials for water desalination

Solar steam generation has garnered significant attention because of its potential to utilize solar energy to collect fresh water. The system comprises several vital components, such as the insulation layer, the photo-thermal layer, and the water supply layer. Among these, the photo-thermal layer plays the most crucial role as it exhibits a high absorption coefficient in the solar spectrum range of 300–2500 nm, allowing for efficient solar-to-thermal conversion. This, in turn, raises the temperature at the liquid–solid interface, leading to water being heated and evaporated. It is worth noting that the effectiveness of solar steam generation depends on the heat transfer and the rate of water evaporation from the liquid–solid interface.

In general, the evaporation of water molecules requires certain energy fluctuations induced by photo-thermal reactions. The absorption energy of water molecules varies based on the intermolecular interaction of different materials. One way to boost evaporation is by weakening the bonding strength between water molecules. To achieve this, Wang *et al.* utilized highly polar units to decorate the interface between the light absorber and water.[109] This causes charge transfer at the solid–liquid interface, leading to interstitial water layers with weak hydrogen bonds between molecules, ultimately promoting evaporation.

Another factor influencing the evaporation process for water desalination is wettability, which influences the transportation of water inside the evaporator and the evaporation process. Porous aero/hydrogels have been demonstrated as efficient materials for solar steam generators due to their versatile porous structure. However, the capillary force is a problem hindering the transportation and evaporation of water. Chen and co-workers balance the capillary force to direct the fluid flow towards the hot region of solar steam generators by using

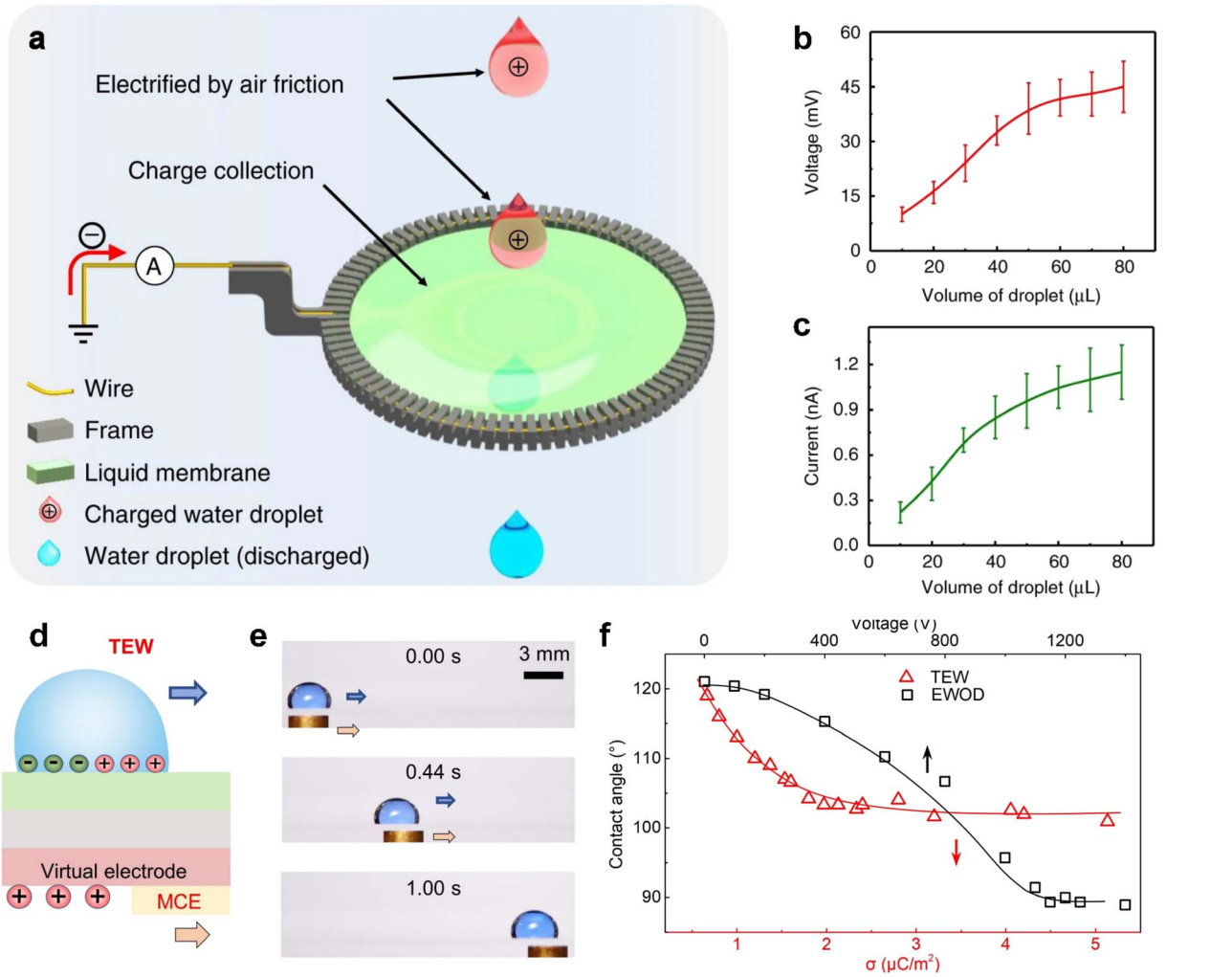

Fig. 11 (a) Schematic illustration of a liquid membrane harvesting energy of falling droplets. (b and c) Open-circuit voltage (VOC) (b) and corresponding short-circuit current (ISC) (c) of droplets moving across the liquid membrane with different sizes. Reproduced with permission.[106] Copyright © 2019 Springer Nature. (d) Typical structures of the EWOD and TEW. (e) Snapshots in time-sequence demonstrate the transportation of a droplet (15 μL) at a constant moving speed of 16.7 mm s^{-1} using a MCE. (f) Correlation between the water CA and SCD. Reproduced with permission.[108] Copyright © 2022 American Association for the Advancement of Science.

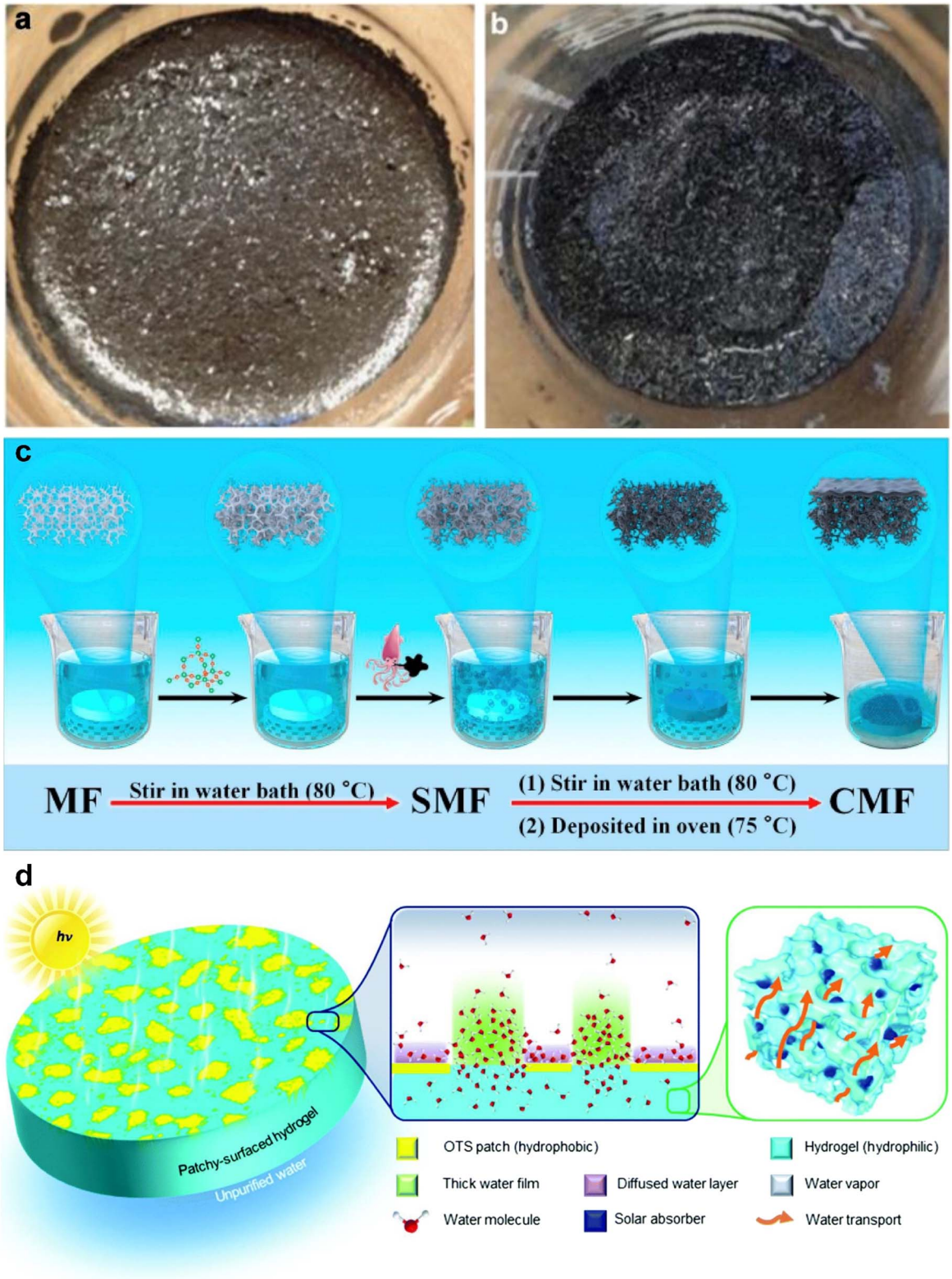

Fig. 12 (a) Graphite flakes form a blanket over the water surface, demonstrating hydrophobicity and poor water penetration. (b) The chemically modified graphite flakes form a water membrane with a low thickness on the surface, showing good water penetration and hydrophilicity. Reproduced with permission.[110] Copyright © 2014 Springer Nature. (c) The preparation sketch of preparation from melamine foam (MF) to composite melamine foam (CMF). Reproduced with permission.[111] Copyright © 2020 Elsevier. (d) Schematic demonstration of promoted solar-driven evaporation enabled by patchy-surface hydrogels and the evaporation mechanism for the hydrophobic island patch integrated hydrophilic surface. Reproduced with permission.[112] Copyright © 2020 Royal Society of Chemistry.

hydrophilic graphite flakes as an interfacial additive.[110] As shown in Fig. 12a and b, water can easily penetrate the graphite foam and reach the surface to promote evaporation. Recently, Li *et al.*[111] filled SiO_2 and ethyl cellulose into superhydrophilic melamine foam to alter the porosity and surface wettability of the melamine foam, as shown in Fig. 12c, which increases the water transport capacity of the device. Guo *et al.* integrated hydrophobic island-shaped patches onto the hydrophilic surface by chemical modification (Fig. 12d).[112] The as-prepared surface demonstrates the following characteristics: (1) a large portion of water is absorbed in the hydrophilic part to gain the thickness of the water film and lead to the inferior impact of the surface on the outermost layer of water molecules, which accelerates evaporation; (2) the hydrophobic parts increase the number of water molecules that diffuse across the water contact lines and thus facilitate the evaporation.

Although the liquid–solid interface is crucial and various strategies have been developed to promote solar steam generation, a systematic study of the function of the solid interface is still needed. Surface modification of the light absorber shows promise in regulating the absorption energy of the liquid, thus contributing to a lower energy barrier for water evaporation. Additionally, the wetting properties of the solid surface are important for the water supply inside the solar steam generation system. Therefore, it is necessary to elucidate the role of the liquid–solid interface and find a way to finely alter the reaction of the interface.

4. Summary and perspectives

In summary, liquid interfaces, including both the liquid–liquid interface and the liquid–solid interface, demonstrate their versatility in various energy conversion and harvesting techniques. Through functionalization of the liquid interface, both the bulk phase and liquid interface can be manipulated to adapt to different reactions, making it a wonderful platform for boosting energy conversion and harvesting. The basic functions of the liquid interface in energy generation/harvesting applications can be categorized into the following aspects:

(1) Segregating layer: in biphasic or multiphasic reaction systems, contact between different phases initiates the mass exchange and even triggers reactions. However, the limited surface area of the interface can regulate the speed of mass exchange or reactant mixing, enabling the reaction rate to be slowed down to a suitable level. Additionally, some reaction products are vulnerable to reactants, but the liquid interface can trap the products in their preferential phase, making it easier to collect them.

(2) Reaction sites: in addition to functioning as a segregating layer, the liquid interface also serves as a reaction site, exhibiting a spatial confinement effect that can limit the reaction to the nanoscale. This offers an opportunity to finely tune the reactions, such as for selective catalysis. It's worth noting that there are two faces to the liquid interface, allowing different reactions to occur simultaneously on each side, which is particularly useful for multiphasic reactions. Furthermore, the interface plays a crucial role in physical reactions, such as ion accumulation and electron transportation, as the reaction can only occur based on the interface, such as in contact electrification.

(3) Stimulus-responsive platform: the liquid–liquid interface is an intriguing platform that can absorb functional NPs. When NPs assemble and become jammed at the interface, the liquid–liquid interface will acquire the properties of the NPs. If the NPs can respond to external stimuli, including magnetic fields, electric fields, or light illumination, the liquid–liquid interface can also be manipulated by the corresponding stimulus. This provides a powerful methodology to manipulate the liquid, which can be further used to control liquid-phase reactions.

Although the liquid interface has shown promising advances and applications in various energy conversion and harvesting techniques, there are still obstacles that need to be addressed. These obstacles can only be overcome by gaining a deeper understanding of the roles of the liquid interface under different application conditions.

First, the liquid–liquid interface remains a complex system, particularly when employing NP self-assembly to alter its properties. The behavior of NPs is influenced by various factors, such as pH, ionic strength, temperature, NPs species, and the nature of the liquid, resulting in NPs forming different textures when jammed at the liquid interface. To manipulate the liquid–liquid interface effectively and accurately, comprehending the kinetics and dynamics of NP self-assembly is critical. Although Chai *et al.* advanced the characterization of the assembly dynamics at the water–oil interface using *in situ* AFM, there are still several unknowns, such as the mechanism of NP attachment and detachment.[113] Therefore, understanding the liquid–liquid interface and the self-assembly of NPs remains essential, and further efforts should focus on employing advanced characterization techniques.

Secondly, the liquid–solid interface has opened up new avenues for energy generation, beyond the traditional techniques of energy conversion, such as catalysis. The recently proposed transistor-inspired configuration for water kinetic energy collection relies on the mass and charge transfer between water and the contacted surface. However, the origin of the charge transfer at both the liquid–solid and liquid–liquid interfaces is still a matter of debate. Researchers have proposed several theories that are specific to their experimental systems. Therefore, further efforts are needed to uncover the underlying mechanism.

Thirdly, it should be noted that most of the energy conversion and harvesting techniques related to liquid interfaces are still in their early stages and have only been demonstrated at the bench-scale level, which is far from practical applications. Therefore, efforts must be made to develop scalable fabrication technologies to enable the production of these technologies on a larger scale for practical power supply purposes.

Author contributions

Y. Chai supervised the project. S. Zhao and Y. Chai wrote the manuscript with input from all coauthors.

Conflicts of interest

There are no conflicts to declare.

Acknowledgements

The authors acknowledge financial support from the National Natural Science Foundation of China (Project no. 22003053), the Research Grants Council of Hong Kong (Project no.21304421), and the Natural Science Foundation of Guangdong Province, China (Project no. 2023A1515011457). The authors also thank OpenAI for editing.

References

1 K. G. Marinova, R. G. Alargova, N. D. Denkov, O. D. Velev, D. N. Petsev, I. B. Ivanov and R. P. Borwankar, *Langmuir*, 1996, **12**, 2045–2051.
2 Y. Zhang, S. E. Feller, B. R. Brooks and R. W. Pastor, *J. Chem. Phys.*, 1995, **103**, 10252–10266.
3 K. Piradashvili, E. M. Alexandrino, F. R. Wurm and K. Landfester, *Chem. Rev.*, 2016, **116**, 2141–2169.
4 S. S. Dukhin, G. Kretzschmar and R. Miller, *Dynamics of Adsorption at Liquid Interfaces: Theory, Experiment, Application*, Elsevier, 1995.
5 H. Sun, L. Li, T. P. Russell and S. Shi, *J. Am. Chem. Soc.*, 2020, **142**, 8591–8595.
6 S. Zhao, J.-Y. Zhang, Y. Fu, S. Zhu, H. C. Shum, X. Liu, Z. Wang, R. Ye, B. Z. Tang, T. P. Russell and Y. Chai, *Nano Lett.*, 2022, **22**, 5538–5543.
7 S. Zhu, G. Xie, H. Cui, Q. Li, J. Forth, S. Yuan, J. Tian, Y. Pan, W. Guo, Y. Chai, Y. Zhang, Z. Yang, R. W. H. Yu, Y. Yu, S. Liu, Y. Chao, Y. Shen, S. Zhao, T. P. Russell and H. C. Shum, *ACS Nano*, 2022, **16**, 13761–13770.
8 W. Mrozik, M. A. Rajaeifar, O. Heidrich and P. Christensen, *Energy Environ. Sci.*, 2021, **14**, 6099–6121.
9 L. Zhou, Y. Tan, J. Wang, W. Xu, Y. Yuan, W. Cai, S. Zhu and J. Zhu, *Nat. Photonics*, 2016, **10**, 393–398.
10 P. Tao, G. Ni, C. Song, W. Shang, J. Wu, J. Zhu, G. Chen and T. Deng, *Nat. Energy*, 2018, **3**, 1031–1041.
11 L. Li, S. Feng, Y. Bai, X. Yang, M. Liu, M. Hao, S. Wang, Y. Wu, F. Sun, Z. Liu and T. Zhang, *Nat. Commun.*, 2022, **13**, 1043.
12 J. Yin, X. Li, J. Yu, Z. Zhang, J. Zhou and W. Guo, *Nat. Nanotechnol.*, 2014, **9**, 378–383.
13 Y. Zhang, R. Ettelaie, B. P. Binks and H. Yang, *ACS Catal.*, 2021, **11**, 1485–1494.
14 I. Hatay, P. Y. Ge, H. Vrubel, X. Hu and H. H. Girault, *Energy Environ. Sci.*, 2011, **4**, 4246–4251.
15 H. C. Shum, A. Bandyopadhyay, S. Bose and D. A. Weitz, *Chem. Mater.*, 2009, **21**, 5548–5555.
16 C. Han, P. Meng, E. R. Waclawik, C. Zhang, X.-H. Li, H. Yang, M. Antonietti and J. Xu, *Angew. Chem., Int. Ed.*, 2018, **57**, 14857–14861.
17 X. Fan, X. Dong, A. C. Karacakol, H. Xie and M. Sitti, *Proc. Natl. Acad. Sci.*, 2020, **117**, 27916–27926.
18 B. B. Yellen, O. Hovorka and G. Friedman, *Proc. Natl. Acad. Sci.*, 2005, **102**, 8860–8864.
19 Y. Wang, S. Gao, W. Xu and Z. Wang, *Adv. Funct. Mater.*, 2020, **30**, 1908252.
20 Q. Zhang, Y. Li, H. Cai, M. Yao, H. Zhang, L. Guo, Z. Lv, M. Li, X. Lu, C. Ren, P. Zhang, Y. Zhang, X. Shi, G. Ding, J. Yao, Z. Yang and Z. L. Wang, *Adv. Mater.*, 2021, **33**, 2105761.
21 J. D. Berry, M. J. Neeson, R. R. Dagastine, D. Y. C. Chan and R. F. Tabor, *J. Colloid Interface Sci.*, 2015, **454**, 226–237.
22 J. Forth, P. Y. Kim, G. Xie, X. Liu, B. A. Helms and T. P. Russell, *Adv. Mater.*, 2019, **31**, 1806370.
23 S. Jain and F. S. Bates, *Science*, 2003, **300**, 460–464.
24 P. Alexandridis, *Curr. Opin. Colloid Interface Sci.*, 1997, **2**, 478–489.
25 P. Mansky, Y. Liu, E. Huang, T. P. Russell and C. Hawker, *Science*, 1997, **275**, 1458–1460.
26 I. Kralova and J. Sjöblom, *J. Dispersion Sci. Technol.*, 2009, **30**, 1363–1383.
27 C. M. O. Lépori, N. M. Correa, J. J. Silber, R. D. Falcone, M. López-López and M. L. Moyá, *Langmuir*, 2019, **35**, 13332–13339.
28 S. De, S. Malik, A. Ghosh, R. Saha and B. Saha, *RSC Adv.*, 2015, **5**, 65757–65767.
29 F. Liang, C. Zhang and Z. Yang, *Adv. Mater.*, 2014, **26**, 6944–6949.
30 R. Deng, H. Li, J. Zhu, B. Li, F. Liang, F. Jia, X. Qu and Z. Yang, *Macromolecules*, 2016, **49**, 1362–1368.
31 B. Liu, W. Wei, X. Qu and Z. Yang, *Angew. Chem., Int. Ed.*, 2008, **47**, 3973–3975.
32 X. Hou, S. Guan, T. Qu, X. Wu, D. Wang, A. Chen and Z. Yang, *ACS Macro Lett.*, 2018, **7**, 1475–1479.
33 M. Cui, T. Emrick and T. P. Russell, *Science*, 2013, **342**, 460–463.
34 Y. Lin, A. Böker, H. Skaff, D. Cookson, A. D. Dinsmore, T. Emrick and T. P. Russell, *Langmuir*, 2005, **21**, 191–194.
35 A. K. Boal, F. Ilhan, J. E. DeRouchey, T. Thurn-Albrecht, T. P. Russell and V. M. Rotello, *Nature*, 2000, **404**, 746–748.
36 S. Shi and T. P. Russell, *Adv. Mater.*, 2018, **30**, 1800714.
37 C. Huang, J. Forth, W. Wang, K. Hong, G. S. Smith, B. A. Helms and T. P. Russell, *Nat. Nanotechnol.*, 2017, **12**, 1060–1063.
38 G. Zhu, B. Peng, J. Chen, Q. Jing and Z. Lin Wang, *Nano Energy*, 2015, **14**, 126–138.
39 C. Xie, Z. Niu, D. Kim, M. Li and P. Yang, *Chem. Rev.*, 2020, **120**, 1184–1249.
40 A. B. D. Cassie, *Discuss. Faraday Soc.*, 1948, **3**, 11–16.
41 Y. Zheng, H. Bai, Z. Huang, X. Tian, F.-Q. Nie, Y. Zhao, J. Zhai and L. Jiang, *Nature*, 2010, **463**, 640–643.
42 Q. Sun, D. Wang, Y. Li, J. Zhang, S. Ye, J. Cui, L. Chen, Z. Wang, H.-J. Butt, D. Vollmer and X. Deng, *Nat. Mater.*, 2019, **18**, 936–941.
43 K. Liu, H. Qi, R. Dong, R. Shivhare, M. Addicoat, T. Zhang, H. Sahabudeen, T. Heine, S. Mannsfeld, U. Kaiser, Z. Zheng and X. Feng, *Nat. Chem.*, 2019, **11**, 994–1000.
44 Y. Lin, A. Böker, J. He, K. Sill, H. Xiang, C. Abetz, X. Li, J. Wang, T. Emrick, S. Long, Q. Wang, A. Balazs and T. P. Russell, *Nature*, 2005, **434**, 55–59.

45 H. Liu, L. Feng, J. Zhai, L. Jiang and D. Zhu, *Langmuir*, 2004, **20**, 5659–5661.
46 S. Wang, X. Feng, J. Yao and L. Jiang, *Angew. Chem., Int. Ed.*, 2006, **45**, 1264–1267.
47 F. Rafieian, M. Hosseini, M. Jonoobi and Q. Yu, *Cellulose*, 2018, **25**, 4695–4710.
48 N. P. Kobayashi, C. L. Donley, S.-Y. Wang and R. S. Williams, *J. Cryst. Growth*, 2007, **299**, 218–222.
49 M. Jin, X. Feng, J. Xi, J. Zhai, K. Cho, L. Feng and L. Jiang, *Macromol. Rapid Commun.*, 2005, **26**, 1805–1809.
50 X. Zhang, Z. Li, K. Liu and L. Jiang, *Adv. Funct. Mater.*, 2013, **23**, 2881–2886.
51 G. Xie, J. Forth, S. Zhu, B. A. Helms, P. D. Ashby, H. C. Shum and T. P. Russell, *Proc. Natl. Acad. Sci.*, 2020, **117**, 8360–8365.
52 S. Zhu, J. Forth, G. Xie, Y. Chao, J. Tian, T. P. Russell and H. C. Shum, *ACS Nano*, 2020, **14**, 11215–11224.
53 C. Huang, Z. Sun, M. Cui, F. Liu, B. A. Helms and T. P. Russell, *Adv. Mater.*, 2016, **28**, 6612–6618.
54 Y. Chai, A. Lukito, Y. Jiang, P. D. Ashby and T. P. Russell, *Nano Lett.*, 2017, **17**, 6453–6457.
55 K. Dietrich, N. Jaensson, I. Buttinoni, G. Volpe and L. Isa, *Phys. Rev. Lett.*, 2020, **125**, 098001.
56 X. Wu, R. Streubel, X. Liu, P. Y. Kim, Y. Chai, Q. Hu, D. Wang, P. Fischer and T. P. Russell, *Proc. Natl. Acad. Sci.*, 2021, **118**, e2017355118.
57 X. Liu, N. Kent, A. Ceballos, R. Streubel, Y. Jiang, Y. Chai, P. Y. Kim, J. Forth, F. Hellman, S. Shi, D. Wang, B. A. Helms, P. D. Ashby, P. Fischer and T. P. Russell, *Science*, 2019, **365**, 264–267.
58 Y. Han, Z. Meng, Y.-X. Ma and C.-F. Chen, *Acc. Chem. Res.*, 2014, **47**, 2026–2040.
59 J. Liu, C. S. Y. Tan and O. A. Scherman, *Angew. Chem., Int. Ed.*, 2018, **57**, 8854–8858.
60 A. Harada, Y. Takashima and M. Nakahata, *Acc. Chem. Res.*, 2014, **47**, 2128–2140.
61 J. J. Rebek, *Chem. Commun.*, 2000, 637–643, DOI: **10.1039/A910339M**.
62 L. Li, H. Sun, M. Li, Y. Yang, T. P. Russell and S. Shi, *Angew. Chem., Int. Ed.*, 2021, **60**, 17394–17397.
63 H. Sun, M. Li, L. Li, T. Liu, Y. Luo, T. P. Russell and S. Shi, *J. Am. Chem. Soc.*, 2021, **143**, 3719–3722.
64 S. Sun, C. Xie, J. Chen, Y. Yang, H. Li, T. P. Russell and S. Shi, *Angew. Chem., Int. Ed.*, 2021, **60**, 26363–26367.
65 Z. Xia, C.-G. Lin, Y. Yang, Y. Wang, Z. Wu, Y.-F. Song, T. P. Russell and S. Shi, *Angew. Chem., Int. Ed.*, 2022, **61**, e202203741.
66 Y. Luo, Y. Yang, Y. Wang, Z. Wu, T. P. Russell and S. Shi, *Angew. Chem., Int. Ed.*, 2022, **61**, e202207199.
67 G. Xie, J. Forth, Y. Chai, P. D. Ashby, B. A. Helms and T. P. Russell, *Chem*, 2019, **5**, 2678–2690.
68 B. Wang, B. Yin, H. Yu, Z. Zhang, G. Wang, S. Shi, X. Gu, W. Yang, B. Z. Tang and T. P. Russell, *ACS Appl. Mater. Interfaces*, 2022, **14**, 54287–54292.
69 B. Qian, S. Shi, H. Wang and T. P. Russell, *ACS Appl. Mater. Interfaces*, 2020, **12**, 13551–13557.
70 S. Shi, B. Qian, X. Wu, H. Sun, H. Wang, H.-B. Zhang, Z.-Z. Yu and T. P. Russell, *Angew. Chem., Int. Ed.*, 2019, **58**, 18171–18176.
71 M. Li, S. Sun, R. Qin, M. Wang, Y. Wang, Y. Yang, Z. Wu and S. Shi, *Soft Matter*, 2023, **19**, 609–614.
72 S. Sun, Y. Luo, Y. Yang, J. Chen, S. Li, Z. Wu and S. Shi, *Small*, 2022, **18**, 2204182.
73 B. Wang, Z. Zhang, W. Feng, J. Luo and S. Shi, *Aggregate*, 2022, **3**, e292.
74 P.-Y. Gu, Y. Chai, H. Hou, G. Xie, Y. Jiang, Q.-F. Xu, F. Liu, P. D. Ashby, J.-M. Lu and T. P. Russell, *Angew. Chem., Int. Ed.*, 2019, **58**, 12112–12116.
75 J. Chen, S. Sun, Y. Wang, W. Feng, Y. Luo, M. Li and S. Shi, *ACS Appl. Mater. Interfaces*, 2023, **15**, 27391–27398.
76 W. Xu, X. Hu, S. Zhuang, Y. Wang, X. Li, L. Zhou, S. Zhu and J. Zhu, *Adv. Energy Mater.*, 2018, **8**, 1702884.
77 R. N. Wenzel, *Ind. Eng. Chem.*, 1936, **28**, 988–994.
78 Q. Zhang, L. He, X. Zhang, D. Tian and L. Jiang, *ACS Nano*, 2020, **14**, 1436–1444.
79 M. Liu, S. Wang and L. Jiang, *Nat. Rev. Mater.*, 2017, **2**, 17036.
80 J. Zhang, J. Wang, Y. Zhao, L. Xu, X. Gao, Y. Zheng and L. Jiang, *Soft Matter*, 2008, **4**, 2232–2237.
81 M. Liu, S. Wang, Z. Wei, Y. Song and L. Jiang, *Adv. Mater.*, 2009, **21**, 665–669.
82 W. Barthlott, T. Schimmel, S. Wiersch, K. Koch, M. Brede, M. Barczewski, S. Walheim, A. Weis, A. Kaltenmaier, A. Leder and H. F. Bohn, *Adv. Mater.*, 2010, **22**, 2325–2328.
83 R. Wang, K. Hashimoto, A. Fujishima, M. Chikuni, E. Kojima, A. Kitamura, M. Shimohigoshi and T. Watanabe, *Nature*, 1997, **388**, 431–432.
84 T.-H. Shen, L. Spillane, J. Peng, Y. Shao-Horn and V. Tileli, *Nat. Catal.*, 2022, **5**, 30–36.
85 X. Hu, W. Xu, L. Zhou, Y. Tan, Y. Wang, S. Zhu and J. Zhu, *Adv. Mater.*, 2017, **29**, 1604031.
86 D. Luo, F. Wang, J. Zhu, F. Cao, Y. Liu, X. Li, R. C. Willson, Z. Yang, C.-W. Chu and Z. Ren, *Proc. Natl. Acad. Sci.*, 2016, **113**, 7711–7716.
87 Z. Song, J. Tang, J. Li and H. Xiao, *Carbohydr. Polym.*, 2013, **92**, 928–933.
88 Z. Xu, Z. Ao, D. Chu, A. Younis, C. M. Li and S. Li, *Sci. Rep.*, 2014, **4**, 6450.
89 Z.-H. Lin, G. Cheng, L. Lin, S. Lee and Z. L. Wang, *Angew. Chem., Int. Ed.*, 2013, **52**, 12545–12549.
90 W. Xu and Z. Wang, *Joule*, 2020, **4**, 2527–2531.
91 W. Xu, H. Zheng, Y. Liu, X. Zhou, C. Zhang, Y. Song, X. Deng, M. Leung, Z. Yang, R. X. Xu, Z. L. Wang, X. C. Zeng and Z. Wang, *Nature*, 2020, **578**, 392–396.
92 F. Wang, M. Liu, C. Liu, Q. Zhao, T. Wang, Z. Wang and X. Du, *Sci. Adv.*, 2022, **8**, eabp9369.
93 Y. Zhang, Z. Huang, Z. Cai, Y. Ye, Z. Li, F. Qin, J. Xiao, D. Zhang, Q. Guo, Y. Song and J. Yang, *Sci. Adv.*, 2021, **7**, eabi7498.
94 A. Li, H. Li, Z. Li, Z. Zhao, K. Li, M. Li and Y. Song, *Sci. Adv.*, 2020, **6**, eaay5808.
95 S. Feng, P. Zhu, H. Zheng, H. Zhan, C. Chen, J. Li, L. Wang, X. Yao, Y. Liu and Z. Wang, *Science*, 2021, **373**, 1344–1348.

96 M. Pera-Titus, L. Leclercq, J.-M. Clacens, F. De Campo and V. Nardello-Rataj, *Angew. Chem., Int. Ed.*, 2015, **54**, 2006–2021.
97 Z. Li, Y. Shi, A. Zhu, Y. Zhao, H. Wang, B. P. Binks and J. Wang, *Angew. Chem., Int. Ed.*, 2021, **60**, 3928–3933.
98 C.-Y. Xie, S.-X. Meng, L.-H. Xue, R.-X. Bai, X. Yang, Y. Wang, Z.-P. Qiu, B. P. Binks, T. Guo and T. Meng, *Langmuir*, 2017, **33**, 14139–14148.
99 Z. Yang, J. Wei, Y. I. Sobolev and B. A. Grzybowski, *Nature*, 2018, **553**, 313–318.
100 S. Crossley, J. Faria, M. Shen and D. E. Resasco, *Science*, 2010, **327**, 68–72.
101 H. Zou, H. Shi, S. Hao, Y. Hao, J. Yang, X. Tian and H. Yang, *J. Am. Chem. Soc.*, 2023, **145**, 2511–2522.
102 J. Yan, M. A. Baird, D. C. Popple, A. Zettl, T. P. Russell and B. A. Helms, *J. Am. Chem. Soc.*, 2022, **144**, 3979–3988.
103 Z. Zhang, X. Li, J. Yin, Y. Xu, W. Fei, M. Xue, Q. Wang, J. Zhou and W. Guo, *Nat. Nanotechnol.*, 2018, **13**, 1109–1119.
104 Z.-H. Lin, G. Cheng, S. Lee, K. C. Pradel and Z. L. Wang, *Adv. Mater.*, 2014, **26**, 4690–4696.
105 J. Xiong, M.-F. Lin, J. Wang, S. L. Gaw, K. Parida and P. S. Lee, *Adv. Energy Mater.*, 2017, **7**, 1701243.
106 J. Nie, Z. Wang, Z. Ren, S. Li, X. Chen and Z. Lin Wang, *Nat. Commun.*, 2019, **10**, 2264.
107 X. Xu, Y. Wang, P. Li, W. Xu, L. Wei, Z. Wang and Z. Yang, *Nano Energy*, 2021, **90**, 106573.
108 W. Xu, Y. Jin, W. Li, Y. Song, S. Gao, B. Zhang, L. Wang, M. Cui, X. Yan and Z. Wang, *Sci. Adv.*, 2022, **8**, eade2085.
109 L. Wang, J. Lin, Y. Li, Y. Yang, X. Liu, Z. Wang, F. Liu, X. Sun, T. Yang, N. Chen and L. Qu, *J. Mater. Chem. A*, 2023, **11**, 7662–7669.
110 H. Ghasemi, G. Ni, A. M. Marconnet, J. Loomis, S. Yerci, N. Miljkovic and G. Chen, *Nat. Commun.*, 2014, **5**, 4449.
111 Z. Li, J. Zhang, S. Zang, C. Yang, Y. Liu, F. Jing, H. Jing, J. Hu, C. Wang and Y. Zhou, *Nano Energy*, 2020, **73**, 104834.
112 Y. Guo, X. Zhao, F. Zhao, Z. Jiao, X. Zhou and G. Yu, *Energy Environ. Sci.*, 2020, **13**, 2087–2095.
113 Y. Chai, J. Hasnain, K. Bahl, M. Wong, D. Li, P. Geissler, P. Y. Kim, Y. Jiang, P. Gu, S. Li, D. Lei, B. A. Helms, T. P. Russell and P. D. Ashby, *Sci. Adv.*, 2020, **6**, eabb8675.